

A Sparse Expansion For Deep Gaussian Processes

Liang Ding ^{a1}, Rui Tuo ^{a2} and Shahin Shahrampour^b

^a Industrial & Systems Engineering, Texas A&M University, College Station, TX

^b Mechanical & Industrial Engineering, Northeastern University, Boston, MA

Abstract

In this work, we use Deep Gaussian Processes (DGPs) as statistical surrogates for stochastic processes with complex distributions. Conventional inferential methods for DGP models can suffer from high computational complexity as they require large-scale operations with kernel matrices for training and inference. In this work, we propose an efficient scheme for accurate inference and efficient training based on a range of Gaussian Processes, called the *Tensor Markov Gaussian Processes* (TMGP). We construct an induced approximation of TMGP referred to as the *hierarchical expansion*. Next, we develop a deep TMGP (DTMGP) model as the composition of multiple hierarchical expansion of TMGPs. The proposed DTMGP model has the following properties: (1) the outputs of each activation function are deterministic while the weights are chosen independently from standard Gaussian distribution; (2) in training or prediction, only $\mathcal{O}(\text{polylog}(M))$ (out of M) activation functions have non-zero outputs, which significantly boosts the computational efficiency. Our numerical experiments on synthetic models and real datasets show the superior computational efficiency of DTMGP over existing DGP models.

Keywords: deep Gaussian processes; Markov Gaussian processes; inducing variables; sparse expansion.

1 Introduction

This work is partially motivated by surrogate modeling of stochastic computer simulations (Ankenman et al., 2010; Plumlee and Tuo, 2014). The ultimate goal in this field is to approximate an underlying stochastic process, defined by a complex stochastic computer simulation code, using a surrogate stochastic process that is computationally efficient. Among existing statistical surrogates, Deep Gaussian Processes (DGP) proposed by Damianou and Lawrence (2013) has recently become a popular choice owing to its exceptional performance and flexibility in fitting the complex distributions from the stochastic processes in real applications (Radaideh and Kozlowski, 2020; Sauer et al., 2022).

DGPs are multi-layer compositions of multi-variate Gaussian Processes (GP). The deep probabilistic structures of DGPs allows a Bayesian formulation to model complex stochastic systems, such as computer vision, natural language processing, etc.. However, the cost of DPGs’ expressiveness and flexibility is the extreme difficulties in training and inference, because the propagation of randomness throughout the layers of DGPs is nonlinear and correlated among layers. Existing approaches for overcoming these difficulties can be separated into two classes – one class focuses on approximating the Bayesian formulations of DGPs, such as variational inference (VI) (Blei et al., 2017), expectation propagation (EP) (Bui et al., 2016), or Vecchia approximation (Sauer et al., 2022), while the other class considers simplified representations of DGPs’ structures, such as inducing-variable approximation (Hensman and Lawrence, 2014) and random Fourier feature expansion (Cutajar et al., 2017).

Simplifications based on inducing variables and random Fourier features (Rahimi and Recht, 2008) partially address the computational issue of DGPs. However, they are still hard to implement. This is because these simplifications of DGPs are deep Neural Networks (DNN) with kernel based activations, correlated random weights and bias parameters, which is equivalent to Bayesian Neural Networks (BNN) (MacKay, 1992; Neal, 1996) with dense and highly correlated structures. Training and inference of these simplifications are at least as hard as existing BNN models.

In this work, we focus on introducing an accurate and efficient simplification of DGPs. We propose a sparse reduced-rank approximation, referred as *Hierarchical Expansion*, for DGPs. Our expansion is specialized for DPGs which are the compositions of multi-variate tensor Markov GPs (TMGP) (Ding and Zhang, 2020), so we call this expanded DGP deep TMGP (DTMGP). One of our main contributions lies in constructing a sparse representation of DGPs. There are only a poly-logarithmic number of activations in our model with non-zero outputs each time we run the model. Because of this sparse property, training of DTMGPs are much faster and easier compared with existing DGP models, avoiding commonly seen numerical issues in training deep models. Another contribution is to show that hierarchical expansion is also highly accurate. Unlike many other GPs/DGPs sparse approximations, the difference between sample paths generated by any DGP and those generated by its hierarchical expansion is small. This property allows DTMGPs to model complex stochastic

systems with satisfactory performance as shown in our numerical experiments.

We use VI to train DTMGP on data generated from simulations and real data and compare it with other existing DGP models. We conduct simulation studies by running experiments on an artificial random field and simulator of a stochastic activity network (Paspachy and Henderson, 2011). We also use the MNIST data set, which is publicly available on the web <http://yann.lecun.com/exdb/mnist/>, to demonstrate the performance of the proposed approach. In these numerical studies, we find that the training process of DTMGP is more stable, and the training loss converges faster compared with its competitors. Besides, we compare the similarities between instances from the underlying systems and instances generated from competing statistical surrogate models. The results show that DTMGP outperforms the alternative DGPs in all experiments.

The remainder of this article is organized as follows. We will review the related literature in Section 2. We introduce general DGP models and an approximation of DGPs called induced approximation in Section 3. The methodology and detailed implementation of DTMGP are introduced in Section 4. Simulation studies are given in Section 5 and experiments on real data are given in 6 . Concluding remarks are made in Section 7. The Appendix includes the required mathematical tools and technical proofs.

2 Literature Review

The state-of-the-art deep learning techniques have brought probabilistic modeling with deep neural network structure in popularity. Based on the concept of deep belief network (DBN) (Hinton et al., 2006), Damianou and Lawrence (2013) generalized the Restricted Boltzmann Machine (Hinton, 2010), which is a DBN with binary output, to deep Gaussian Processes based on Gaussian process mapping. DGPs have been a popular tool in several applications. Their prowess has been demonstrated on many classification tasks (Damianou and Lawrence, 2013; Fei et al., 2018; Yang and Klabjan, 2021). Compared with traditional DNNs, the flexibility in uncertainty quantification of DGPs makes them ideal candidate for surrogate modeling (Radaideh and Kozlowski, 2020; Sauer et al., 2022). DGPs are commonly used statistical surrogates in many applications such as Bayesian optimization (Hebbal et al., 2021), calibration (Marmin and Filippone, 2022), multi-fidelity analysis (Ko and Kim, 2021),

healthcare (Li et al., 2021), and etc.

However, training and inference of DGPs are difficult. Current attempts can be separated into two classes. One focuses on designing more efficient and accurate training algorithm while the other one on constructing DGP architectures with sparsity. Efficient training and inference algorithms include expectation propagation (Bui et al., 2016), doubly stochastic variational inference (Salimbeni and Deisenroth, 2017), stochastic gradient Hamiltonian Monte Carlo (Havasi et al., 2018), elliptical slice sampling (Sauer et al., 2022), Vecchia approximation (Vecchia, 1988; Sauer et al., 2022; Katzfuss and Guinness, 2021), and etc. Reformulation of DGPs to simplified models is an alternative approach. DGPs are reformulated as an variational model in Tran et al. (2016). Low-rank approximations for GPs in Banerjee et al. (2008); Cressie and Johannesson (2008) are also extended to DGPs. Hensman and Lawrence (2014); Dai et al. (2016) extend the inducing-variable method to DGPs. Cutajar et al. (2017) uses random Fourier feature expansion to show that DGPs are equivalent to infinitely wide BNN with corresponding activations.

In this work, we consider DGPs with Markov structure and, based on the Markov structure, we design an accurate and efficient sparse expansion for DGPs. Sidén and Lindsten (2020) proposes compositions of *discrete* Gaussian Markov random field on graph and called deep graphical models of this structure *Deep Gaussian Markov Random Fields* (DGMRF). We must point out that our DTMGPs is essentially different from DGMRF because DTMGPs are *not* deep graphical models. More specifically, DGMRF treats every activation as a random variable and imposes a graphical Markov structure on these activations, i.e., any two non-adjacent randomly distributed activations are conditionally independent given all other activations. On the other hand, every activation in DTMGP is one of the orthonormal basis functions of a *continuous* Gaussian Markov random field and these orthonormal basis functions constitute a so-called *hierarchical expansion* of the field.

3 General DGP Models

3.1 Deep Gaussian Processes

A GP \mathcal{G} is a random function characterized by its mean function μ and covariance function k . To be more specific, given any input \mathbf{x} , the output $\mathcal{G}(\mathbf{x})$ has a Gaussian distribution

with mean $\mu(\mathbf{x})$ and variance $k(\mathbf{x}, \mathbf{x})$, and given any pair of inputs \mathbf{x} and \mathbf{x}' , the covariance between $\mathcal{G}(\mathbf{x})$ and $\mathcal{G}(\mathbf{x}')$ is $k(\mathbf{x}, \mathbf{x}')$:

$$\begin{aligned}\mathcal{G}(\mathbf{x}) &\sim \mathcal{N}(\mu(\mathbf{x}), k(\mathbf{x}, \mathbf{x})), \\ \mathbf{Cov}(\mathcal{G}(\mathbf{x}), \mathcal{G}(\mathbf{x}')) &= k(\mathbf{x}, \mathbf{x}').\end{aligned}\tag{1}$$

A W -variate GP is simply a W -vector of GPs $[\mathcal{G}_1, \mathcal{G}_2, \dots, \mathcal{G}_W]$. Without loss of generality, we assume that any multivariate GP in the following content has mean function $\mu = 0$ and independently distributed entries. A H -layer DGP $\mathbf{f}^{(H)}$ is then the composition of H multi-variate GPs:

$$\mathbf{f}^{(H)}(\mathbf{x}^*) = \mathcal{G}^{(H)} \circ \dots \circ \mathcal{G}^{(2)} \circ \mathcal{G}^{(1)}(\mathbf{x}^*),\tag{2}$$

where $f \circ g$ denotes the composition function $f(g(\cdot))$, $\mathcal{G}^{(h)}$ denotes a $W^{(h)}$ -variate GP $[\mathcal{G}_1^{(h)}, \mathcal{G}_2^{(h)}, \dots, \mathcal{G}_{W^{(h)}}^{(h)}]$, and $W^{(h)}$ is called the width of layer h . The formulation (2) of DGP can be viewed as a DNN with random activations $\{\mathcal{G}_i^{(h)}\}$.

While DGP yields a non-parametric and Bayesian formulation of DNNs, computations for inference/prediction of DGPs are cumbersome. For example, given a set of input-output pairs $(\mathbf{X}, \mathbf{Y}) \in \mathbb{R}^{n \times d} \times \mathbb{R}^n$, the conditional probability distribution $\mathbb{P}(\mathbf{Y}|\mathbf{X})$ induced by (2) is

$$\mathbb{P}(\mathbf{Y}|\mathbf{X}) = \int \mathbb{P}(\mathbf{Y}|\mathbf{f}^{(H)})\mathbb{P}(\mathbf{f}^{(H-1)}|\mathbf{f}^{(H-2)}) \dots \mathbb{P}(\mathbf{f}^{(1)}|\mathbf{X})d\mathbf{f}^{(1)} \dots d\mathbf{f}^{(H)},\tag{3}$$

where $\mathbf{f}^{(h)}$ denotes the output vector from layer h :

$$\mathbf{f}^{(h)} = \mathcal{G}^{(h)} \circ \mathcal{G}^{(h-1)} \circ \dots \circ \mathcal{G}^{(1)},$$

with $h = 1, \dots, H$. Evidently, the integral (3) is intractable, leading to the intractability of inference and predictions of DGP $\mathbf{f}^{(H)}$ conditioned on any observed data (\mathbf{X}, \mathbf{Y}) .

3.2 Induced Approximation of DGPs

The inference of GP, which acts as a single activation in DGP, is also time and space consuming. A challenge for GPs lies in their computational complexity and storage for the inverse of covariance matrix $k(\mathbf{X}, \mathbf{X})$ which are $\mathcal{O}(n^3)$ and $\mathcal{O}(n^2)$, respectively, when the covariance matrix is of size n . To alleviate this computational problem, current methods, such as inducing-variable approximation in Hensman and Lawrence (2014); Dai et al. (2016)

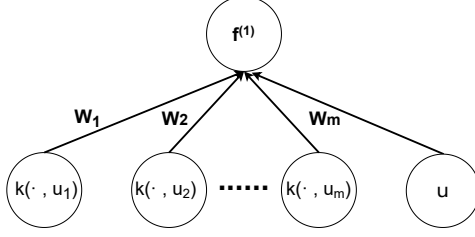


Figure 1: Induced approximation $\hat{\mathcal{G}}$ can be represented as a one-layer neural network with correlated Gaussian distributed weights $\mathbf{w} = [k(\mathbf{U}, \mathbf{U})]^{-1}\mathcal{G}(\mathbf{U})$ and bias μ .

and random Fourier feature approximation in Cutajar et al. (2017), focus on approximating the covariance matrix $k(\mathbf{X}, \mathbf{X})$ by some low rank matrices.

Instead of approximating the covariance matrix, we approximate the GP activations in a DGP directly. In the following content, we will construct a reduced-rank approximation called induced approximation. Induced approximation can bring a more flexible and clear deep neural network representation of DGPs.

Without loss of generality, let \mathcal{G} defined in (1) be a GP with constant mean μ and covariance function k . Inspired by the kriging method (Matheron, 1963; Sacks et al., 1989), we can approximate GP \mathcal{G} defined in (1) by the following finite-rank approximation:

$$\hat{\mathcal{G}}(\mathbf{x}^*) := \mu + k(\mathbf{x}^*, \mathbf{U})[k(\mathbf{U}, \mathbf{U})]^{-1}\mathcal{G}(\mathbf{U}) \quad (4)$$

where we call $\mathbf{U} = \{\mathbf{u}_i \in \mathbb{R}^d\}_{i=1}^m$ the inducing points and $\mathcal{G}(\mathbf{U})$ are the values of \mathcal{G} on \mathbf{U} . According to theory in (Ritter, 2000; Wang et al., 2020; Ding and Zhang, 2020), the required number of inducing points for achieving the optimal statistical error is much lower than the sample size, provided that the inducing points \mathbf{U} are well-chosen. Hence, (4) can be computed in a highly efficient way.

Finite-rank approximation (4) can be represented as a one-layer neural network with correlated Gaussian distributed weights $\mathbf{w} = [k(\mathbf{U}, \mathbf{U})]^{-1}\mathcal{G}(\mathbf{U})$ and bias μ as shown in Figure 1. However, the correlated Gaussian distributed weights still make training and inference difficult. In order to write the finite-rank approximation (4) in the form of a neural network with independently distributed weights, we can simply apply Cholesky decomposition on kernel matrix $k(\mathbf{U}, \mathbf{U})$, which leads to the following equation:

$$\hat{\mathcal{G}}(\mathbf{x}^*) = \mu + k(\mathbf{x}^*, \mathbf{U})R_{\mathbf{U}}^{-1}\mathbf{Z} := \mu + \phi^T(\mathbf{x}^*)\mathbf{Z}, \quad (5)$$

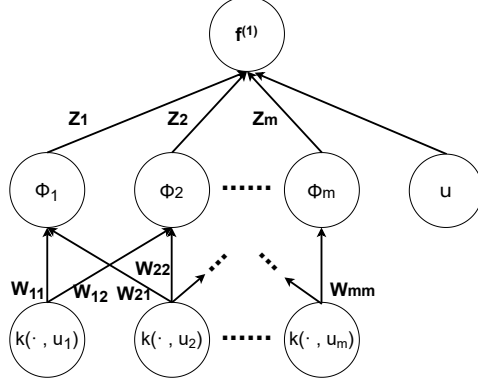


Figure 2: A two-layer neural network representation of $\hat{\mathcal{G}}$ with deterministic weights $\mathbf{W} = [R_{\mathbf{U}}^T]^{-1}$, i.i.d. standard Gaussian weights \mathbf{Z} , and bias μ .

where $R_{\mathbf{U}}$ is the Cholesky decomposition of matrix $k(\mathbf{U}, \mathbf{U})$ and $\mathbf{Z} = [R_{\mathbf{U}}^T]^{-1}\mathcal{G}(\mathbf{U}) \in \mathbb{R}^m$ are i.i.d. distributed standard Gaussian random variables. We call approximation (5) induced approximation and Figure 2 shows that induced approximation can be represented as a two-layer neural network where functions ϕ act as an extra hidden layer. Because the approximation (5) consists of only m Gaussians, the time and space complexity for its inference are then reduced to $\mathcal{O}(m^2n)$ and $\mathcal{O}(mn)$, respectively.

The induced approximation of a DGP is to approximate each random activation by corresponding induced approximation. For example, suppose that in a DGP $\mathbf{f}^{(H)}$, all activations in the same layer are characterized by the same covariance function $k^{(h)}$. Then, the induced approximation $\tilde{\mathbf{f}}^{(H)}$ of $\mathbf{f}^{(H)}$ is

$$\begin{aligned} \tilde{\mathbf{f}}^{(H)}(\mathbf{x}^*) &= [\mathbf{Z}^{(H)}\phi^{(H)}(\cdot) + \boldsymbol{\mu}^{(H)}] \circ \dots \circ [\mathbf{Z}^{(1)}\phi^{(1)}(\mathbf{x}^*) + \boldsymbol{\mu}^{(1)}], \\ [\phi^{(h)}(\cdot)]^T &= k^{(h)}(\cdot, \mathbf{U}^{(h)})R_h^{-1} \quad \text{for } h = 1, \dots, H \end{aligned} \tag{6}$$

where, for $h = 1, \dots, H$, $\mathbf{Z}^{(h)} \in \mathbb{R}^{W^{(h)} \times m^{(h)}}$ is a matrix with i.i.d. standard Gaussian entries, $\mathbf{U}^{(h)}$ are the total $m^{(h)}$ inducing variables for kernel $k^{(h)}$, $R_h \in \mathbb{R}^{m^{(h)} \times m^{(h)}}$ is the Cholesky decomposition of the covariance matrix $k^{(h)}(\mathbf{U}^{(h)}, \mathbf{U}^{(h)})$, and $\boldsymbol{\mu}^{(h)} \in \mathbb{R}^{W^{(h)}}$ is the mean vector and can be treated as the bias of layer h .

In the next section, we will show that if kernel k is in a class of kernel function called tensor Markov kernel and inducing points \mathbf{U} are a specific design called sparse grid, then induced approximations (5) and (6) can be further written as a sparse approximation.

4 Methodology of DTMGP

In this section, we first introduce the concept of TMGPs. We then introduce hierarchical expansion of TMGPs and how it leads to mutually orthogonal feature functions with hierarchical supports. Based on hierarchical expansion, we can introduce the implementation and training of DTMGPs.

4.1 Tensor Markov GPs

Hierarchical expansion is applied to a class of GPs called tensor Markov GP. In one dimension, a Markov GP is characterized by the following Lemma in Marcus and Rosen (2006):

Lemma 1 (Marcus and Rosen (2006) Lemma 5.1.8). *Let $I \subseteq \mathbb{R}$. Let \mathcal{G} be a zero mean GP defined on I with continuous positive definite kernel k . Then, \mathcal{G} is a Markov GP and k is Markov kernel if and only if there exist positive functions p and q on I with p/q strictly increasing such that*

$$k(x, x') = p(\min(x, x'))q(\max(x, x')), \quad x, x' \in I. \quad (7)$$

For any Markov GP \mathcal{G} we have that, conditioned on its distribution at a point x , its distributions at any point $x_l < x$ and any point $x_u > x$ are independent: $\mathcal{G}(x_l) \perp \mathcal{G}(x_u) | \mathcal{G}(x)$, whence Markov GP. Markov GPs have two advantages in computations. Firstly, given any ordered inducing points $\{u_1 < \dots < u_n\}$, the distribution of $\mathcal{G}(x)$ at any x , where $u_i < x < u_{i+1}$, depends only on its left and right inducing points $\mathcal{G}(u_i)$ and $\mathcal{G}(u_{i+1})$. Secondly, for any induced approximation, accuracy of the approximation at x only depends on the distances between x and its left and right neighbors, respectively. Therefore, evenly distributed inducing variables can achieve an accurate approximation that is also cheap to compute.

To generalize one-dimensional Markov GP to higher dimensions, we can take the tensor product of d one-dimensional Markov GPs to construct a GP in d dimension:

Definition 1. *A GP is called TMGP if and only if it is a zero mean GP with covariance function of the form*

$$k(\mathbf{x}, \mathbf{x}') = \prod_{j=1}^d k_j(x_j, x'_j), \quad (8)$$

with Markov kernel k_j for $j = 1, \dots, d$. A kernel of the form (8) is called *tensor Markov kernel (TMK)*.

Example 1. Commonly used TMKs include Laplace kernel $k(\mathbf{x}, \mathbf{x}') = \exp(\sum_{j=1}^d \theta_j |x_j - x'_j|)$ and Brownian sheet kernel $k(\mathbf{x}, \mathbf{x}') = \prod_{j=1}^d (1 + \theta_j \min\{x_j, x'_j\})$.

Similar to its one-dimensional counterpart, we want to construct an accurate approximation of TMGP with the smallest possible number of inducing variables. The challenge is to define properly the “left”, and “right” neighbors on a multidimensional space, analogously to the real line. This leads us to the hierarchical expansion, described next.

4.2 Hierarchical Expansion

To construct the hierarchical expansion, we let inducing variables \mathbf{U} be an experimental design \mathbf{X}_l^{SG} called level- l *Sparse Grid (SG)* (Bungartz and Griebel, 2004; Plumlee, 2014), where level l determines the number of inducing variables. Furthermore, the SG inducing variables must be sorted in a specific order. Detailed introduction of SGs and the required order are provided in Appendix A, and MATLAB codes for generating SGs satisfying the requirement can be found in the *Sparse Grid Designs* package (Plumlee, 2021). Examples of two-dimensional SGs are shown in Figure 3. From the examples, we can see that the incremental points from the next level of a SG exhibit a hierarchical structure – higher level SG consists of local SGs of smaller levels.

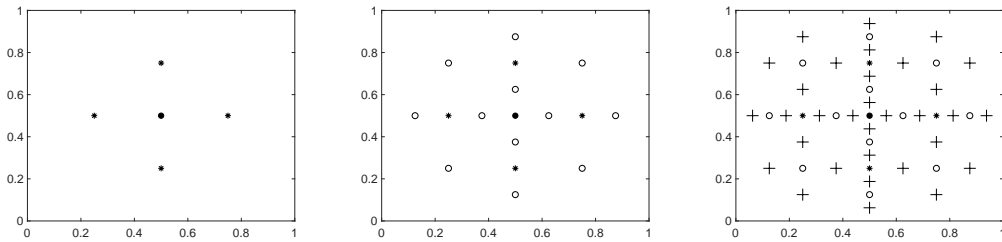


Figure 3: Two-dimensional level-2 SG (left), level-3 SG (middle) and level-4 SG (right) on cube $(0, 1)^2$. The incremental points from the second level, third level and fourth level are labeled by *, o and +, respectively.

Hierarchical expansion of a TMGP \mathcal{G} with inducing points \mathbf{X}_l^{SG} is then simply:

$$\mathcal{G}(\mathbf{x}^*) \approx k(\mathbf{x}^*, \mathbf{X}_l^{\text{SG}}) R_l^{-1} \mathbf{Z} := \boldsymbol{\phi}^T(\mathbf{x}^*) \mathbf{Z}, \quad (9)$$

where $k(\mathbf{x}^*, \mathbf{X}_l^{\text{SG}}) = [k(\mathbf{x}^*, \mathbf{x}_1), \dots, k(\mathbf{x}^*, \mathbf{x}_{m_l})]$ is the covariance vector, $k(\mathbf{X}_l^{\text{SG}}, \mathbf{X}_l^{\text{SG}}) = [k(\mathbf{x}_i, \mathbf{x}_j)]_{i,j \leq m_l}$ is the covariance matrix, R_l is the Cholesky decomposition of $k(\mathbf{X}_l^{\text{SG}}, \mathbf{X}_l^{\text{SG}})$, $\mathbf{Z} = [Z_1, \dots, Z_{m_l}]$ are i.i.d. standard Gaussian random variables and $\phi = [\phi_i]_{i=1}^{m_l}$ are called hierarchical features. Hierarchical expansion (9) yields a sparse approximation of TMGP that is easy to compute as shown in the following theorems.

Theorem 1. *The number of non-zero entries on R_l^{-1} is $\mathcal{O}(m_l)$ and R_l^{-1} can be computed in $\mathcal{O}(m_l)$ operations.*

Theorem 2. *Given any input point \mathbf{x}^* , the number of non-zero entries on the vector of hierarchical features $\phi(\mathbf{x}^*)$ is $\mathcal{O}([\log m_l]^{2d-1})$.*

The algorithm for computing R_l^{-1} in $\mathcal{O}(m_l)$ operations is given in Appendix B, and proofs for Theorems 1 and 2 are provided in supplementary material. Since we can compute R_l^{-1} in $\mathcal{O}(m_l)$ operations and the numbers of non-zero entries on R_l^{-1} is $\mathcal{O}(m_l)$, hierarchical expansion can be computed in $\mathcal{O}(m_l)$ operations. Moreover, if matrix R_l^{-1} is given, because the numbers of non-zero entries on $\phi(\mathbf{x}^*)$ is only $\mathcal{O}([\log m_l]^{2d-1})$, the computational time of the hierarchical expansion can be further reduced to $\mathcal{O}([\log m_l]^{2d-1})$. The sparsity of hierarchical feature vector ϕ relies on the fact that the supports of $\{\phi_i\}_{i=1}^{m_l}$ are either nested or disjoint and, hence, form a hierarchical structure as shown in Figure 4.

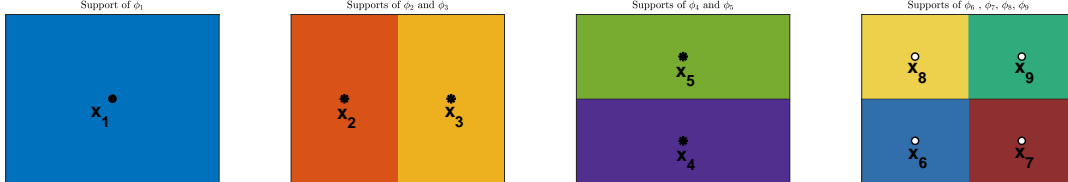


Figure 4: Support of hierarchical feature ϕ_1 corresponding to \mathbf{x}_1 in level 1 (left); supports of $\{\phi_i\}_{i=2}^5$ corresponding to $\{\mathbf{x}_i\}_{i=2}^5$ (middle figures); supports of $\{\phi_i\}_{i=6}^9$ corresponding to $\{\mathbf{x}_i\}_{i=6}^9$ in level 3 (right).

\mathbf{X}_l^{SG} is also regarded as the index set of ϕ , because instead of labeling each hierarchical feature by number i , we can also label it by the corresponding inducing variable $\mathbf{x}_i \in \mathbf{X}_l^{\text{SG}}$. As shown in Figure 5, for any i , \mathbf{x}_i is the only point at which ϕ_i is not differentiable along all dimensions. Hence, we call \mathbf{x}_i the center of ϕ_i . From this perspective, we can claim that, given any \mathbf{x}^* , the distribution of the approximation at \mathbf{x}^* only depends on

$\mathcal{O}([\log m_l]^{2d-1})$ inducing variables. As a result, the hierarchical expansion generalizes the one-dimensional Markov property while still remaining a high accuracy approximate. We discuss the approximation error of hierarchical expansion in supplementary material.

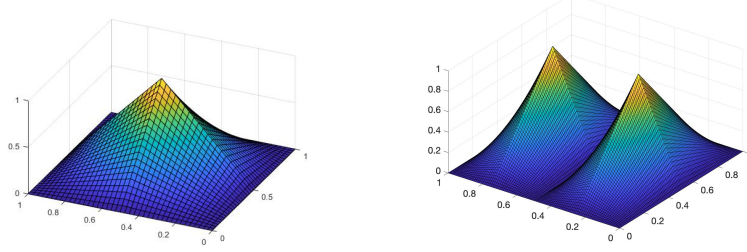


Figure 5: Hierarchical features ϕ_1 (left) and ϕ_2, ϕ_3 (right) generated by the tensor Brownian Bridge kernel $k(\mathbf{x}, \mathbf{x}') = \prod_{j=1}^2 \min\{x_j, x'_j\}(1 - \max\{x_j, x'_j\})$.

The following numerical example illustrates the sparsity of hierarchical expansion:

Example 2. Let two-dimensional TMK $k(\mathbf{x}, \mathbf{x}') = \exp\{-\sum_{j=1}^2 |x_j - x'_j|\}$. Let

$$\mathbf{X}_2^{\text{SG}} = \left[\left(\frac{1}{2}, \frac{1}{2} \right), \left(\frac{1}{2}, \frac{1}{4} \right), \left(\frac{1}{2}, \frac{3}{4} \right), \left(\frac{1}{4}, \frac{1}{2} \right), \left(\frac{3}{4}, \frac{1}{2} \right) \right],$$

be the sorted level-2 SG. Then, we numerically compute the inverse Cholesky decomposition R_2^{-1} and we get

$$R_2^{-1} = \begin{bmatrix} 1.0000 & -1.2416 & -1.2416 & -1.2416 & -1.2416 \\ 0 & 1.5942 & 0.0000 & 0.0000 & 0.0000 \\ 0 & 0 & 1.5942 & 0.0000 & 0.0000 \\ 0 & 0 & 0 & 1.5942 & 0.0000 \\ 0 & 0 & 0 & 0 & 1.5942 \end{bmatrix}.$$

Let $\mathbf{x}_1^* = (0.8147, 0.9058)$, and $\mathbf{x}_2^* = (0.2785, 0.5469)$ be two randomly chosen points. We numerically compute the hierarchical features at \mathbf{x}_1^* and \mathbf{x}_2^* and we get

$$\begin{aligned} k(\mathbf{x}_1^*, \mathbf{X}_2^{\text{SG}})R_2^{-1} &= [0.4865, 0, 0.3918, 0.0000, 0.3918], \\ k(\mathbf{x}_2^*, \mathbf{X}_2^{\text{SG}})R_2^{-1} &= [0.7646, 0.5291, 0, 0, 0.0933]. \end{aligned}$$

As we can see, matrix R_2^{-1} is sparse and each of $k(\mathbf{x}_1^*, \mathbf{X}_2^{\text{SG}})R_2^{-1}$ and $k(\mathbf{x}_2^*, \mathbf{X}_2^{\text{SG}})R_2^{-1}$ has two zero elements. The sparsity is even more visible as the number of inducing points increases.

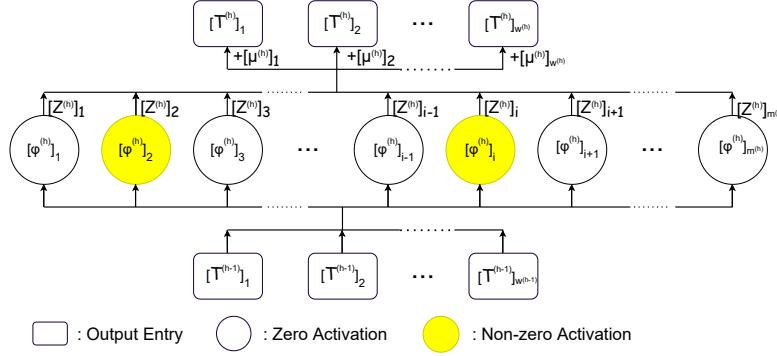


Figure 6: Only $\mathcal{O}([\log m^{(h)}]2^{W^{(h-1)}}-1)$ activations are non-zero in layer h of DTMGP $\mathcal{T}^{(H)}$.

4.3 Deep Tensor Markov GPs

A H -layer DTMGP $\mathcal{T}^{(H)}$ is defined as the composition of H hierarchical expansions of multi-variate TMGP:

$$\mathcal{T}^{(H)}(\mathbf{x}^*) = [\mathbf{Z}^{(H)}\phi^{(H)}(\cdot) + \boldsymbol{\mu}^{(H)}] \circ \dots \circ [\mathbf{Z}^{(1)}\phi^{(1)}(\mathbf{x}^*) + \boldsymbol{\mu}^{(1)}], \quad (10)$$

where, for $h = 1, \dots, H$, $\mathbf{Z}^{(h)}$ is a $W^{(h)}$ -by- $m^{(h)}$ matrix with i.i.d. standard Gaussian entries, $W^{(h)}$ is the dimension of the output (width of the neural network) of layer h , $m^{(h)}$ is the number of hierarchical features for approximating a $W^{(h)}$ -variate TMGP, $\phi^{(h)}$ consists of the $m^{(h)}$ hierarchical features for approximating the TMGP, acting as the activation functions in layer h , and $\boldsymbol{\mu}^{(h)} \in \mathbb{R}^{W^{(h)}}$ is the parameterized mean for the TMGP in layer h .

Let us now focus on layer h of $\mathcal{T}^{(H)}$ to compare DTMGP with DNN. Let $\mathcal{T}^{(h)} = (\mathcal{T}_1^{(h)}, \dots, \mathcal{T}_{W^{(h)}}^{(h)})$ denote the $W^{(h)}$ -dimensional output of layer h . We then have the following structure:

$$\mathcal{T}^{(h-1)} \rightarrow \underbrace{(\phi_1^{(h)}(\mathcal{T}^{(h-1)}), \dots, \phi_{m^{(h)}}^{(h)}(\mathcal{T}^{(h-1)}))}_{\# \text{ non-zero entries: } \mathcal{O}([\log m^{(h)}]2^{W^{(h-1)}}-1)} \rightarrow \left[\mathcal{T}_j^{(h)} = \mu_j^{(h)} + \sum_{i=1}^{m^{(h)}} Z_{j,i} \phi_i^{(h)}(\mathcal{T}^{(h-1)}) \right]_{j=1}^{W^{(h)}},$$

where $\phi_i^{(h)}(\mathcal{T}^{(h-1)})$ is the i^{th} entry of vector $k^{(h)}(\mathcal{T}^{(h-1)}, \mathbf{X}_{l^{(h)}}^{\text{SG}})[R^{(h)}]^{-1}$, $k^{(h)}$ is the TMK for layer h , $\mathbf{X}_{l^{(h)}}^{\text{SG}}$ is a level- $l^{(h)}$ SG of size $m^{(h)}$ for induced approximation, and $R^{(h)}$ is the Cholesky decomposition of covariance matrix $k^{(h)}(\mathbf{X}_{l^{(h)}}^{\text{SG}}, \mathbf{X}_{l^{(h)}}^{\text{SG}})$. This structure is also illustrated in Figure 6.

If we treat DTMGP as a DNN, then, for $h = 1, \dots, H$, layer h is equipped with $m^{(h)}$ activations $\{k^{(h)}(\cdot, \mathbf{x}) : \mathbf{x} \in \mathbf{X}_{l^{(h)}}^{\text{SG}}\}$, a sparse linear filter $[R^{(h)}]^{-1}$ which converts the dense input to sparse local hierarchical features, bias $\boldsymbol{\mu}^{(h)}$, and i.i.d. standard Gaussian weights. Moreover, sparse linear filters $\{[R^{(h)}]^{-1}\}_{h=1}^H$ are fixed for a specific hierarchical expansion. Therefore, $\{[R^{(h)}]^{-1}\}_{h=1}^H$ can be computed and stored in advance. Due to Theorems 1 and 2, the space complexity for storing $\{[R^{(h)}]^{-1}\}_{h=1}^H$ is linear in the number of inducing points and the time complexity of any operation in layer h of DTMGP is $\mathcal{O}([\log m^{(h)}]^{2W^{(h-1)}-1})$.

4.4 Variational Inference

The proposed DTMGP is mathematically equivalent to a deep neural network with biases $\{\boldsymbol{\mu}^{(h)}\}_{h=1}^H$ and independently and normally distributed weights $\{\mathbf{Z}^{(h)}\}_{h=1}^H$. So we can parameterize DTMGP as a BNN with independently and normally distributed weights. Specifically, we regard the variances and means of all Gaussian weights, and the biases as parameters of the BNN. A DTMGP can be represented as a stochastic process $f_{\boldsymbol{\theta}}$ in the parameterized family $\mathcal{F}_{\boldsymbol{\Theta}}$:

$$\mathcal{F}_{\boldsymbol{\Theta}} = \left\{ \left[(\boldsymbol{\Sigma}^{(H)} \odot \mathbf{Z}^{(H)} + \mathbf{m}^{(H)})\phi^{(H)} + \boldsymbol{\mu}^{(H)} \right] \circ \dots \circ \left[(\boldsymbol{\Sigma}^{(1)} \odot \mathbf{Z}^{(1)} + \mathbf{m}^{(1)})\phi^{(1)} + \boldsymbol{\mu}^{(1)} \right] : \right. \\ \left. \{ \boldsymbol{\Sigma}^{(h)}, \mathbf{m}^{(h)}, \boldsymbol{\mu}^{(h)} \}_{h=1}^H \in \boldsymbol{\Theta} \right\},$$

where $\boldsymbol{\Theta}$ denotes the set of parameters

$$\boldsymbol{\Theta} := \left\{ \boldsymbol{\Sigma}^{(h)} \in \mathbb{R}_+^{W^{(h)} \times m^{(h)}}, \mathbf{m}^{(h)} \in \mathbb{R}^{W^{(h)} \times m^{(h)}}, \boldsymbol{\mu}^{(h)} \in \mathbb{R}^{W^{(h)}}, h = 1, \dots, H \right\},$$

and $A \odot B$ denotes the entry-wise multiplication of matrices A and B , i.e., the Hadamard product. In other words, the family $\mathcal{F}_{\boldsymbol{\Theta}}$ consists of BNNs with activations $\{\phi^{(h)}\}_{h=1}^H$, parameterized biases, and normally distributed weights.

Given observations (\mathbf{X}, \mathbf{Y}) , our goal is to search for the parameters $\boldsymbol{\theta}^*$ that maximizes the marginal likelihood $\mathbb{P}(\mathbf{Y}|\mathbf{X}, \boldsymbol{\theta})$. The DTMGP $f_{\boldsymbol{\theta}^*}$ can best interpret how (\mathbf{X}, \mathbf{Y}) is generated. Computing $\mathbb{P}(\mathbf{Y}|\mathbf{X}, \boldsymbol{\theta})$ of any DGP involves intractable integral as shown in (3), but we can obtain a tractable lower bound using VI. VI first assigns a prior $f_{\tilde{\boldsymbol{\theta}}}$ with some $\tilde{\boldsymbol{\theta}} = \{\tilde{\boldsymbol{\Sigma}}^{(h)}, \tilde{\mathbf{m}}^{(h)}, \tilde{\boldsymbol{\mu}}^{(h)}\}_{h=1}^H$ to the underlying stochastic process generating (\mathbf{X}, \mathbf{Y}) and then maximizes the following *evidence lower bound* (ELBO):

$$\mathcal{E}(\boldsymbol{\theta}) = \mathbb{E}_{f_{\boldsymbol{\theta}}} [\log \Pr(\mathbf{Y}|\mathbf{X}, \boldsymbol{\theta})] - \mathcal{D}_{KL}(f_{\boldsymbol{\theta}} \| f_{\tilde{\boldsymbol{\theta}}}), \quad (11)$$

which is the lower bound of log-likelihood $\log \Pr(\mathbf{Y}|\mathbf{X}, \boldsymbol{\theta})$.

In our framework, the term $\mathbb{E}_{f_{\boldsymbol{\theta}}}[\log \Pr(\mathbf{Y}|\mathbf{X}, \boldsymbol{\theta})]$ is called the *negative energy* and can be explicitly written as

$$\mathbb{E}_{f_{\boldsymbol{\theta}}}[\log \Pr(\mathbf{Y}|\mathbf{X}, \boldsymbol{\theta})] = \mathbb{E}_{\mathbf{Z}^{(1)}, \dots, \mathbf{Z}^{(H)}}[\log \Pr(\mathbf{Y}|\mathbf{X}, \mathbf{Z}^{(1)}, \dots, \mathbf{Z}^{(H)}, \boldsymbol{\theta})].$$

This term now can be efficiently estimated by stochastic optimization based on Monte Carlo methods, such as doubly-stochastic approximation (Hensman and Lawrence, 2014; Dai et al., 2014; Salimbeni and Deisenroth, 2017). The term $\mathcal{D}_{KL}(f_{\boldsymbol{\theta}}\|f_{\tilde{\boldsymbol{\theta}}})$ is the *KL-divergence* between $f_{\boldsymbol{\theta}}$ and the prior $f_{\tilde{\boldsymbol{\theta}}}$ and it can be explicitly written

$$\mathcal{D}_{KL}(f_{\boldsymbol{\theta}}\|f_{\tilde{\boldsymbol{\theta}}}) = \frac{1}{2} \sum_{h=1}^H \sum_{i=1}^{W^{(h)}} \sum_{j=1}^{m^{(h)}} \frac{|[\mathbf{m}^{(h)}]_{i,j} - [\tilde{\mathbf{m}}^{(h)}]_{i,j}|^2}{[\tilde{\boldsymbol{\Sigma}}^{(h)}]_{i,j}^2} + \frac{[\boldsymbol{\Sigma}^{(h)}]_{i,j}^2}{[\tilde{\boldsymbol{\Sigma}}^{(h)}]_{i,j}^2} - 1 - \log \frac{[\boldsymbol{\Sigma}^{(h)}]_{i,j}^2}{[\tilde{\boldsymbol{\Sigma}}^{(h)}]_{i,j}^2}.$$

The computation of \mathcal{E} is efficient at any $\boldsymbol{\theta} \in \boldsymbol{\Theta}$, the training process of DTMGP is simply defined as

$$\boldsymbol{\theta}^* = \arg \max_{\boldsymbol{\theta} \in \boldsymbol{\Theta}} \{ \mathbb{E}_{f_{\boldsymbol{\theta}}}[\log \Pr(\mathbf{Y}|\mathbf{X})] - \mathcal{D}_{KL}(f_{\boldsymbol{\theta}}\|f_{\tilde{\boldsymbol{\theta}}}) \}. \quad (12)$$

This optimization problem can also be treated as a penalized regression problem where the negative energy term is the model fitness level and the KL-divergence term is the penalty of being far from the DTMGP prior. Equation (12) can be solved efficiently by using the automatic differentiation technique (Neidinger, 2010; Baydin et al., 2018).

5 Simulation Studies

In this section, we run simulations on systems with stochastic outputs to access DTMGP's capacity in modeling stochastic processes. More specifically, in each experiment, output Y of the underlying system at each input \mathbf{x} follows an *unknown* distribution $F(\cdot|\mathbf{x})$:

$$Y(\mathbf{x}) \sim F(y|\mathbf{x}).$$

A training set $(\mathbf{X}_{\text{train}}, \mathbf{Y}_{\text{train}})$ is independently collected where $\mathbf{Y}_{\text{train}} = Y(\mathbf{X}_{\text{train}})$ is the realization of the underlying system on inputs $\mathbf{X}_{\text{train}}$. We then train competing models using training set $(\mathbf{X}_{\text{train}}, \mathbf{Y}_{\text{train}})$.

Let $\hat{Y}(\cdot)$ denote a trained model. We first choose a test set \mathbf{X}_{test} from the input space. For each input $\mathbf{x} \in \mathbf{X}_{\text{test}}$, we sample 100 independent realizations from the true underlying

system and from the trained model to get data sets $\{Y_i(\mathbf{x})\}_{i=1}^{100}$ and $\{\hat{Y}_i(\mathbf{x})\}_{i=1}^{100}$, respectively. We then use the two-sample *Kolmogorov-Smirnov* (KS) statistic:

$$D_{\mathbf{x}} = \sup_y \left| \frac{1}{100} \sum_{i=1}^{100} \mathbf{1}_{\{Y_i(\mathbf{x}) \leq y\}} - \frac{1}{100} \sum_{i=1}^{100} \mathbf{1}_{\{\hat{Y}_i(\mathbf{x}) \leq y\}} \right|$$

to quantify the similarity between Y and \hat{Y} on input \mathbf{x} . The smaller $D_{\mathbf{x}}$ is, the closer the two distributions are. We assess the overall performance of $\hat{Y}(\cdot)$ via the following averaged two-sample KS statistic over test set \mathbf{X}_{test} :

$$D = \frac{1}{|\mathbf{X}_{\text{test}}|} \sum_{\mathbf{x} \in \mathbf{X}_{\text{test}}} D_{\mathbf{x}}.$$

We repeat each experiment R times and call each a macro-replication from which we obtain D_r , $r = 1, \dots, R$. Finally, we report the mean and standard deviation

$$\begin{aligned} \bar{D} &= \frac{1}{R} \sum_{r=1}^R D_r, \\ \hat{\sigma} &= \left[\frac{1}{R} \sum_{r=1}^R \left(D_r - \bar{D} \right)^2 \right]^{1/2}. \end{aligned}$$

In all experiments, activations of DTMGP are hierarchical features generated from TMGPs with the Laplace covariance function $k(\mathbf{x}, \mathbf{x}') = \exp\{-\frac{\|\mathbf{x} - \mathbf{x}'\|_1}{d}\}$ and we set prior of all the weights as standard normal random variables: $[\tilde{\Sigma}^{(h)}]_{i,j} = 1$, $[\tilde{\mathbf{m}}^{(h)}]_{i,j} = 0$ for all i, j, h . We compare DTMGP with the following existing models:

1. **GP**: standard Gaussian process with squared exponential covariance function. This model can be interpreted as an infinitely-wide BNN with one hidden layer (Neal, 1996).
2. **BNN-ReLU** (Schmidt et al., 1992; Graves, 2011; Blundell et al., 2015): ReLU deep neural networks (Glorot et al., 2011) with parameterized Gaussian distributed weights and biases. The ReLU with standard Gaussian distributed weights and biases are treated as the prior. Then the VI method is applied to search the BNN that can maximize the ELBO defined in (11).
3. **DGP-RFF** (Cutajar et al., 2017): A Random Fourier feature expansion of DGP with each layer represented by Gaussian processes with the Gaussian kernel $\exp\{-\sum_{j=1}^d w_j |x_j -$

$x'_j|^2\}$. DGP-RFF can be viewed as a BNN with Gaussian distributed weights and activations of the form $\cos(\Omega^T \mathbf{x} + b)$ where Ω is a Gaussian distributed vector and b has a uniform distribution on $[0, 2\pi]$. DGP-RFF is trained with VI approximation provided in Cutajar et al. (2017).

Note that DTMGP, BNN-ReLU, and DGP-RFF can all be represented by BNNs. The difference among these BNNs lies in the activations and the connectivity pattern between layers. Therefore, for each data set, we adopt the same architectures of the equivalent BNNs for fair comparisons. In other words, except for the specific activations and connections, all deep models are in terms of BNNs with equal number of layers, widths, weights, and biases. In all experiments, we use VI to train all the competing deep models and use the standard Bayes rule to get the posterior of the standard GP.

We conduct experiments with two simulation models: a two-dimensional non-Gaussian random field in Section 5.1, and the expected revenue of a 13-dimensional Stochastic Activity Network problem in Section 5.2.

All the experiments are implemented in MATLAB 2021 with DEEP LEARNING TOOLBOX on a computer with macOS, 3.3 GHz Intel Core i5 CPU, and 8 GB of RAM (2133Mhz).

5.1 A Non-Gaussian Random Field

In this section, we use the following non-Gaussian and non-stationary random field in two dimensions to assess the sample and computational efficiency of the proposed methodology:

$$Y(\mathbf{x}) = \frac{1}{1 + \exp\{B(\mathbf{x})\}}, \quad \mathbf{x} \in [0, 1]^2$$

where $B(\mathbf{x})$ is a *Brownian sheet*, which is defined as a zero-mean GP with covariance function $\prod_{d=1}^2 (1 + \min\{x_d, x'_d\})$.

In this experiment, $\mathbf{X}_{\text{train}}$ is randomly collected from the cube $[0, 1]^2$ and $\mathbf{Y}_{\text{train}}$ is from independently sample paths of $B(\mathbf{x})$ on $\mathbf{X}_{\text{train}}$. We investigate the performance of each method as the sizes of the training set $(\mathbf{X}_{\text{train}}, \mathbf{Y}_{\text{train}})$ increase. For each training set, we randomly select $n_{\text{test}} = 100$ points from $[0, 1]^2$ as the test set, denoted as \mathbf{X}_{test} . We run $R = 20$ macro-replications and compute \hat{D} and the associated standard deviation $\hat{\sigma}$ for each method.

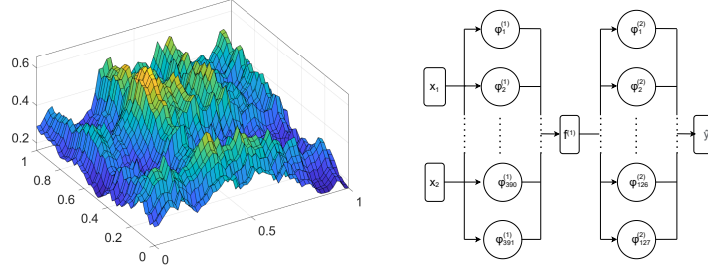


Figure 7: A sample path of non-Gaussian random field $\frac{1}{1+\exp\{B(\mathbf{x})\}}$. Right: architecture shared by all BNNs to capture the random field.

All the competing models in this experiment share the following architecture:

$$\hat{Y}(\mathbf{x}) = \sum_{i=1}^{127} Z_i^{(2)} \phi_i^{(2)} \left(\sum_{j=1}^{181} Z_j^{(1)} \phi_j^{(1)}(\mathbf{x}) \right)$$

where $\{Z_i^{(h)}\}$ are i.i.d. Gaussian random variables with parametrized means $\{\mu_i^{(h)}\}$ and standard deviation $\{\sigma_i^{(h)}\}$ and $\{\phi_i^{(h)}\}$ are the activations. In DTMGP, $\{\phi_i^{(h)}\}$ are hierarchical features; in BNN, $\{\phi_i^{(h)}\}$ are parametrized ReLU activations; in DGP-RFF, $\{\phi_i^{(h)}\}$ are randomly generated Fourier features. Such an architecture is in the form $f^{(2)} \circ f^{(1)}$, which is consistent with the target random field.

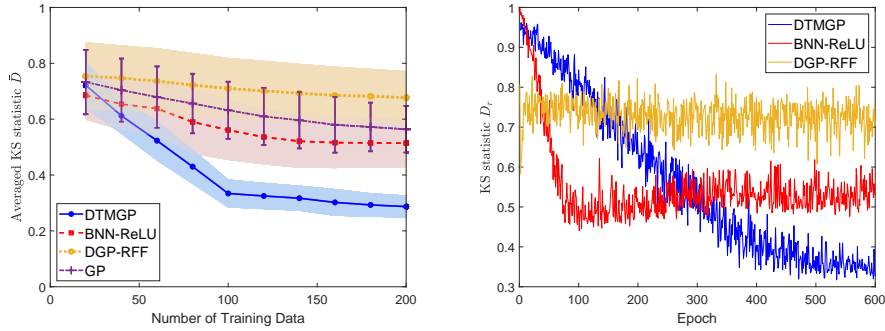


Figure 8: Left: \bar{D} of each model, the shaded areas represent one standard deviation $\hat{\sigma}$ of all deep GPs and the error bars represent one standard deviation of the GP. Right: D_r of each model changes with epoch during training for sample size $n = 100$.

Figure 8 shows averaged KS statistics \bar{D} and how D_r changes in each epoch for sample size $n = 100$. When sample size n exceeds 60, DTMGP significantly outperforms all its competitors in simulating the target random field and its advantage tends to be more

prominent as the sample size increases. As shown in the case sample size $n = 100$, training of BNN-ReLU takes smallest number of epochs and it converges to the steady state fast. This is because ReLU activations have the simplest form. However, the simple form of ReLU activations also makes BNN-ReLU hard to reconstruct the real underlying random field. Training of DTMGP takes relatively more epochs. This is because the hierarchical features in DTMGPs are more flexible compared with ReLU activations. The flexibility of hierarchical features, meanwhile, can help DTMGP capture more information from the training data. We omit the training process of standard GP models because the posteriors are computed directly.

5.2 Stochastic Activity Network

In this subsection, we consider the stochastic activity network (SAN) where the arcs are labeled from 1 through 13. The detailed explanation of SAN is available in Avramidis and Wilson (1996). As shown in the left of Figure 9, each arc i in the SAN is associated with a task with random duration D_i and task durations are mutually independent. Suppose that D_i is exponentially distributed with mean X_i for each i . Suppose that we can control $X_i > 0$ for each i , but there is an associated cost. In particular, the overall cost is defined as

$$C(\mathbf{X}) = T(\mathbf{X}) + f(\mathbf{X})$$

where $\mathbf{X} = (X_1, \dots, X_{13})$, $T(\mathbf{X})$ is the (random) duration of the longest path from a to i, and $f(\mathbf{X}) = \sum_{i=1}^{13} X_i^{-1}$. The closed form of $C(\mathbf{X})$ is unknown, however, MATLAB simulator of this problem is available in the SimOpt library (Pasupathy and Henderson, 2011).

In this experiment, data are collected from a maximin Latin hypercube design (LHD) that maximizes the minimum distance between points (van Dam et al., 2007). The LHD consists of 5000 sample points from the cube $[0.5, 5]^{13}$. At each sample point, we run m simulation replications with $m = 2, 4, \dots, 20$. The simulation output is stochastic and has an unknown variance. In order to select reasonable prior for the target stochastic process, we first normalize all the output so that all output data in the training set and testing set are distributed on $[0, 1]$. We then run $m = 10$ replications at each design point during the training process to estimate the variance at each point. Based on the sample estimates, we

let the i.i.d. prior of each coefficient in our BNNs be normal distributed with mean zero and variance 0.04.

We examine the performance of each method as the number of replications m increase. Given m , we construct the test set \mathbf{X}_{test} of size $n_{\text{test}} = 100$ by random samples from $[0.5, 5]^{13}$. We compute \hat{D} of each method, its associated standard deviation $\hat{\sigma}$ based on $R = 20$ macro-replications.

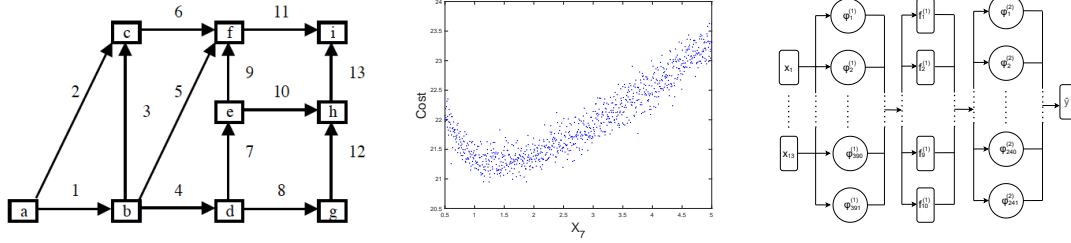


Figure 9: Left: structure of SAN. Middle: i.i.d. samples of $C(\mathbf{X})$ with $X_i = 2.5$, $i \neq 7$ and $X_7 \in [0.5, 5]$. Right: architecture shared by all competing deep GPs to capture $C(\mathbf{X})$.

Similar to section 5.1, all the competing models in this experiment share the following architecture:

$$\hat{Y}(\mathbf{x}) = \sum_{i=1}^{241} Z_i^{(2)} \phi_i^{(2)} \left(\sum_{j=1}^{391} Z_{1,j}^{(1)} \phi_j^{(1)}(\mathbf{x}), \sum_{j=1}^{391} Z_{2,j}^{(1)} \phi_j^{(1)}(\mathbf{x}), \dots, \sum_{j=1}^{391} Z_{10,j}^{(1)} \phi_j^{(1)}(\mathbf{x}) \right)$$

with $Z_{i,j}^{(h)} \sim \mathcal{N}(0, 0.04)$ for any i, j, h . In general, all BNNs can be treated as three-layer deep GPs where the first hidden layer consists of ten GPs and the second hidden layer consists of one GP. Moreover, GPs in the first hidden layer are linear combinations of 391 activation functions and GP in the second hidden layer is linear combination of 241 activation functions. Such an architecture is flexible enough to capture the random process $C(\mathbf{X})$.

Figure 10 shows the averaged KS statistics \bar{D} and how D_r changes in each epoch when the number of replications $m = 10$ at each design point. The total number of training data is $5000m$ with $m = 2, 4, \dots, 20$. Here we exclude the GP models as a competing method because the standard GP regression package cannot handle such a big data set. For all $m = 2, 4, \dots, 20$, DTMGP significantly outperforms all its competitors in simulating the target stochastic process and its advantage tends to be more prominent as m increases. Figure 10 also shows the training processes of all competing deep GPs. The result is similar

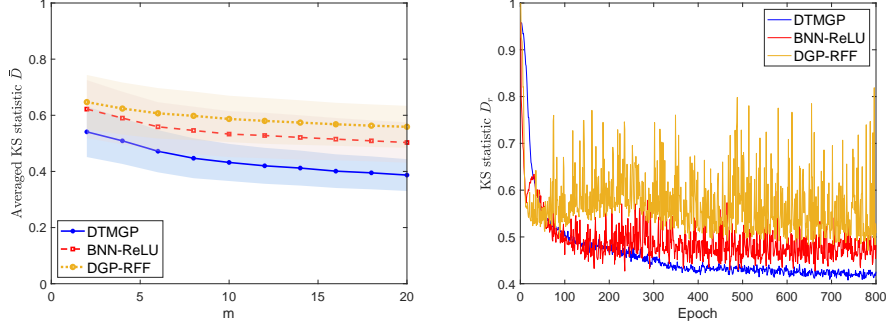


Figure 10: Left: \bar{D} of each model, the shaded areas represent one standard deviation $\hat{\sigma}$ of all deep GPs and the error bars represent one standard deviation of the GP. Right: D_r of each model changes with epoch during training for $m = 10$ replications.

to the previous artificial random field experiment. The only difference is that DTMGP is more stable compared with BNN-ReLU and DGP-RFF. We believe that it is the sparsity of DTMGP that improves the stability of its training.

6 Experiment on Real Data

In this section we examine the performance of the proposed methodology on a real data set. We use the MNIST dataset (Deng, 2012) and consider training DGP models on conditional generative problem. The MNIST dataset consists of $n = 60000$ data pairs $(\mathbf{X}, \mathbf{Y}) = \{(\mathbf{x}_i, \mathbf{y}_i)\}_{i=1}^n$ where, for any $i = 1, \dots, n$, input $\mathbf{x}_i \in \{0, 1, \dots, 9\}$ is a digit from zero to nine and outputs \mathbf{y}_i is the 28-by-28 image of a hand-written x_i . We aim at using the Bayesian formula to train a generative model conditioned on the input \mathbf{x} . Given an input \mathbf{x} in a specific digit class, the trained model should generate a random matrix output that is similar to data \mathbf{Y} in the same class. To summarize, the generative problem can be treated as a stochastic process $Y(\mathbf{x}) \in \mathbb{R}^{28 \times 28}$ with $\mathbf{x} \in \{0, 1, \dots, 9\}$ and our goal is to use deep GP model to reconstruct $Y(\cdot)$ from observed data.

We compare DTMGP with BNN-ReLU and DGP-RFF introduced in section 5. We omit GP model because the data size is beyond its capacity. All competing deep GP models share the following architecture. We first apply the word embedding technique on input \mathbf{x} , which uses a linear transformation A to map discrete input $\mathbf{x} \in \{0, 1, \dots, 9\}$ to a 100-dimensional

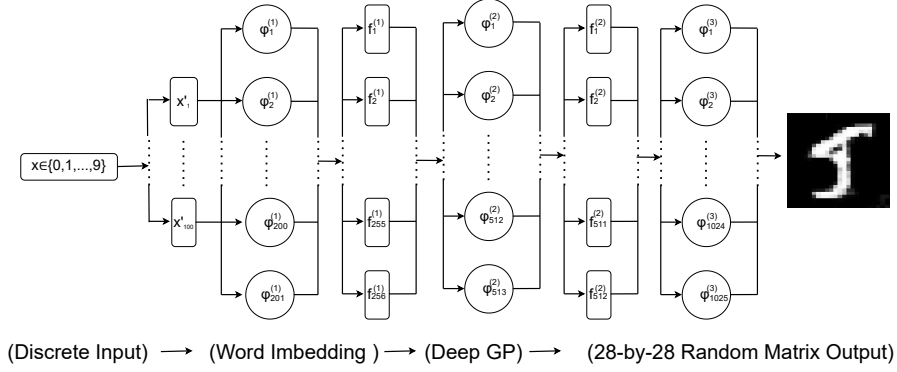


Figure 11: All competing deep GPs share the same architecture.

vector $\mathbf{x}' \in \mathbb{R}^{100}$. We then adopt a 4-layer BNN architecture where \mathbf{x}' is the input layer, the first hidden layer consists of 201 activations and a 256-dimensional output, the second hidden layer consists of 513 activations and a 512-dimensional output, and the third hidden layer consists of 1025 activations and the final output is 28-by-28 random matrix. In specific, the architecture can be written as:

$$\begin{aligned}
 f_j^{(1)} &= \sum_{i=1}^{201} Z_{i,j}^{(1)} \phi_i^{(1)}(A\mathbf{x}), \quad j = 1, \dots, 256, \quad Z_{i,j}^{(1)} \sim \mathcal{N}(0, 1), \quad A \in \mathbb{R}^{100 \times 1}, \\
 f_j^{(2)} &= \sum_{i=1}^{513} Z_{i,j}^{(2)} \phi_i^{(2)}(f_1^{(1)}, \dots, f_{256}^{(1)}), \quad j = 1, \dots, 512, \quad Z_{i,j}^{(2)} \sim \mathcal{N}(0, 1), \\
 \hat{Y}_{l,j} &= \sum_{i=1}^{1025} Z_{i,l,j}^{(3)} \phi_i^{(3)}(f_1^{(2)}, \dots, f_{512}^{(2)}), \quad l, j = 1, \dots, 28, \quad Z_{i,l,j}^{(3)} \sim \mathcal{N}(0, 1).
 \end{aligned}$$

Figure 11 illustrates the above architecture.

We use all 60000 samples from the MNIST dataset to train DTMGP and its competitors BNN-RELU and DGP-RFF. We train the models by mini-batch SGD and, in each epoch, we sample their random outputs at input \mathbf{x} , for $\mathbf{x} = 0, \dots, 9$. Because the output in this experiment is 28-by-28 random matrix and we have no way to sample data from the real distribution of MNIST, the previous KS statistics does not apply. Given that the output random matrix is, in fact, hand-written digit, we can directly check the outputs of each model to evaluate their performances.

Conditional samples generated by DTMGP, BNN-ReLU, and DGP-RFF at the 10th, 20th, 30th, and 40th are shown in the left of Figure 12. It is obvious that, DTMGP generates

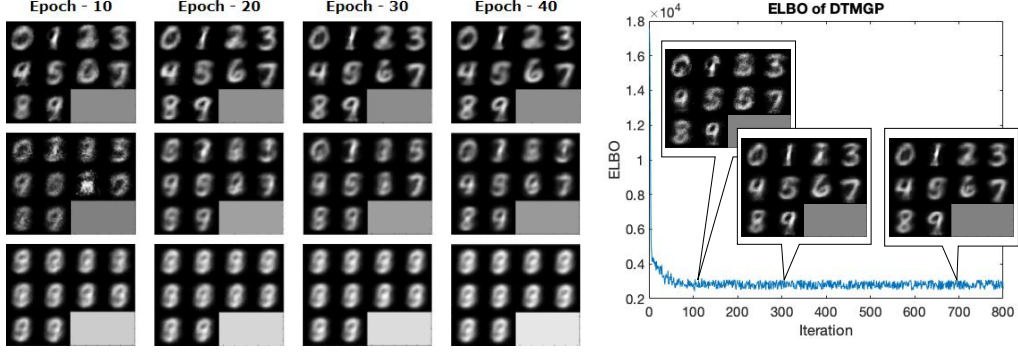


Figure 12: Left: Conditional samples from DTMGP (top row), BNN-ReLU (middle row), and DGP-RFF (bottom row) at the 10th, 20th, 30th, 40th epoch during training. Right: ELBO of DTMGP at each iteration during training

conditional sample similar to the true data and has the best performance, DGP-RFF fails to reconstruct the conditional samples and has the worst performance. This is because, similar to experiments in simulation studies, the hierarchical features of DTMGP can help capturing the local features of the hand-written digits while the cosine activations of DGP-RFF do not have the ability of capturing local features.

BNN-ReLU successfully reconstructs some, but not all, conditional samples. Compared with DTMGP, its performance is unstable. This is because the number of parameters in BNN-ReLU is much higher than that of DTMGP, which leads to an unstable training process. Instead, as shown in the right of Figure 12, the ELBO of DTMGP converges to a stable level after the 100th iteration (the 5th epoch) and, hence, the conditional samples generated by DTMGP converge after the 5th epoch.

Range of y -axis in the ELBO plot cannot fully reflect the training efficiency of a model because the ELBO value depends on many factor, such as the prior, the activations and architecture chosen, and even the distribution of data. On the other hand, the rate of convergence of ELBO and its fluctuation during training can reflect the efficiency stability of DTMGP. Fast convergence of ELBO indicates that the model can be trained in a small number of iterations and small fluctuation of ELBO indicates that performance of the model is reliable on different portions of the data. Therefore, training of DTMGP is efficient and stable because of the sparsity of DTMGP.

7 Conclusions and Discussion

We use hierarchical features to expand DGPs which are composition of TMGPs and we call this expansion DTMGP. Our expansion is easy to compute and leads to a sparse representation of DGPs. Because the supports of hierarchical features are either nested or disjoint and exhibit a hierarchical structure, only a poly-logarithmic number of activations throughout a DTMGP have non-zero output conditioned on any input or operation. Also, hierarchical features can accurately and efficiently capture local features from inputs. This property of hierarchical features enables DTMGP to have high performance in both prediction problems and generative problems as shown in our numerical experiments. Compared with existing DGP models, inference and training of DTMGP is efficient thanks to its sparsity while instances generated from DTMGP are also relatively accurate under the KS test.

The current paper can potentially be extended in several ways. Firstly, how to apply hierarchical expansion on DGPs with more general structures, such as DGPs with Matérn covariance functions, can be studied in future research. Secondly, it was pointed out by Stein (2014) that, approximating the likelihood function of GP by low-rank methods, such as inducing point and random features, may have an adverse effect on the performance. How large this effect is for the proposed DGP models should be studied in further investigation.

Appendix

A Sparse Grid Designs with Required Order

The class of SG adopted in this work is called *Hyperbolic-cross* SG, which is the union of full grids (FG) with dyadic structures. Without loss of generality, we can assume that all design points are collected from the hypercube $(0, 1)^d$, and we start constructing SGs satisfying the required order with the one-dimensional case, which is also called dyadic point set.

A one-dimensional level- l dyadic point set \mathbf{X}_l with increasing order is simply defined as $\mathbf{X}_l = \{2^{-l}, 2 \cdot 2^{-l}, \dots, 1 - 2^{-l}\}$. However, this order cannot result in a sparse representation of hierarchical expansion. We need to sort the points according to their levels. Firstly, given a level $l \in \mathbb{N}$, we define the following set consisting only of odd numbers:

$$\boldsymbol{\rho}(l) = \{1, 3, 5, \dots, 2^l - 1\}.$$

Then given a level- l dyadic point set \mathbf{X}_l and a level- $(l-1)$ dyadic point set \mathbf{X}_{l-1} , we can define the sorted incremental set

$$\mathbf{D}_l = \mathbf{X}_l - \mathbf{X}_{l-1} = \{i2^{-l} : i \in \rho(l)\},$$

with $\mathbf{D}_0 = \emptyset$. It is straightforward to check that

$$\mathbf{X}_l = \bigcup_{\ell=1}^l \mathbf{D}_\ell, \quad \mathbf{D}_l \cap \mathbf{D}_k = \emptyset, \text{ if } l \neq k.$$

For any incremental set \mathbf{D}_l , we can label any point in \mathbf{D}_l by $x_{l,i}$, $i \in \rho(l)$ so that the label is unique for any point: $x_{l,i} \neq x_{l',i'}$ if and only if $(l,i) \neq (l',i')$. Now we can define the following dyadic set with the required order:

$$\mathbf{X}_l^* = [\mathbf{D}_1, \mathbf{D}_2, \dots, \mathbf{D}_l] = [x_{\ell,i} : \ell \leq l, i \in \rho(\ell)].$$

For example, $\mathbf{X}_3^* = [\frac{1}{2}, \frac{1}{4}, \frac{3}{4}, \frac{1}{8}, \frac{3}{8}, \frac{5}{8}, \frac{7}{8}]$ with $\mathbf{D}_1 = [\frac{1}{2}]$, $\mathbf{D}_2 = [\frac{1}{4}, \frac{3}{4}]$, and $\mathbf{D}_3 = [\frac{1}{8}, \frac{3}{8}, \frac{5}{8}, \frac{7}{8}]$, respectively.

We also define the Cartesian product of one-dimensional sorted \mathbf{X}_l^* 's for later use in Algorithms and proofs. We call this sorted Cartesian product full grid (FG) $\mathbf{X}_\mathbf{l}^*$ labeled by $\mathbf{l} = (l_1, \dots, l_d) \in \mathbb{N}^d$:

$$\mathbf{X}_\mathbf{l}^* = \bigotimes_{j=1}^d \mathbf{X}_{l_j}^* = [(x_{\ell_1, i_1}, x_{\ell_2, i_2}, \dots, x_{\ell_d, i_d}) : \ell_j \leq l_j, i_j \in \rho(\ell_j), j = 1, \dots, d].$$

For simplicity, we define the Cartesian product $\rho(\mathbf{l}) = \times_{j=1}^d \rho(l_j)$ for any $\mathbf{l} \in \mathbb{N}^d$ so that any points in $\mathbf{X}_\mathbf{l}^*$ can be represented as $\mathbf{x}_{\mathbf{l}, \mathbf{i}} = (x_{l_1, i_1}, x_{l_2, i_2}, \dots, x_{l_d, i_d})$ for any $\mathbf{l} \in \mathbb{N}^d$ and $\mathbf{i} \in \rho(\mathbf{l})$. Then we have a more compact representation of $\mathbf{X}_\mathbf{l}^*$:

$$\mathbf{X}_\mathbf{l}^* = [\mathbf{x}_{\ell, \mathbf{i}} : \ell \leq \mathbf{l}, \mathbf{i} \in \rho(\ell)].$$

For example, the sorted FG $\mathbf{X}_{(1,2)}^*$ is

$$\mathbf{X}_{(1,2)}^* = [(\frac{1}{2}, \frac{1}{2}), (\frac{1}{2}, \frac{1}{4}), (\frac{1}{2}, \frac{3}{4})].$$

Finally, a level- l SG satisfying our required order is the union of sorted FGs as follows:

$$\mathbf{X}_l^{\text{SG}} = \bigcup_{|\mathbf{l}|=l+d-1} \mathbf{X}_\mathbf{l}^* = [\mathbf{x}_{\mathbf{l}, \mathbf{i}} : |\mathbf{l}| \leq l, \mathbf{i} \in \rho(\mathbf{l})],$$

where $|\mathbf{l}|$ denote the l_1 norm $\sum_{j=1}^d |l_j|$. To be more specific, a point $\mathbf{x}_{\mathbf{l},\mathbf{i}} \in \mathbf{X}_l^{\text{SG}}$ must be ahead of any $\mathbf{x}_{\mathbf{l}'}$ with $|\mathbf{l}'| > |\mathbf{l}|$. For example, the two-dimensional sorted SG \mathbf{X}_2^{SG} is

$$\mathbf{X}_2^{\text{SG}} = \left[\underbrace{\left(\frac{1}{2}, \frac{1}{2}\right)}_{\text{level } |(1,1)|=2}, \underbrace{\left(\frac{1}{2}, \frac{1}{4}\right), \left(\frac{1}{2}, \frac{3}{4}\right)}_{\text{level } |(1,2)|=3}, \underbrace{\left(\frac{1}{4}, \frac{1}{2}\right), \left(\frac{3}{4}, \frac{1}{2}\right)}_{\text{level } |(2,1)|=3} \right].$$

Unlike FG, whose size increases exponentially in dimension d , the size of SGs increases relatively mildly in d . Lemma 3.6 in Bungartz and Griebel (2004) stipulates that the sample size of a d -dimensional level- l \mathbf{X}_l^{SG} is given by

$$|\mathbf{X}_l^{\text{SG}}| = \sum_{\ell=0}^{l-1} 2^\ell \binom{\ell + d - 1}{d - 1} = 2^l \cdot \left(\frac{l^{d-1}}{(d-1)!} + \mathcal{O}(l^{d-2}) \right) = \mathcal{O}(2^l l^{d-1}). \quad (13)$$

B Algorithms

We first introduce how to compute R^{-1} , with R the Cholesky decomposition of $k(\mathbf{X}_l^*, \mathbf{X}_l^*)$, k is a one-dimensional Markov kernel and \mathbf{X}_l^* is a one-dimensional sorted level- l dyadic point set. To present the algorithm for computing the inverse of Cholesky decomposition, we also label the entries on matrices by points in \mathbf{X}_l^* . For example, $[R^{-1}]_{x,x'}$ represents entry with row index corresponding to point $x \in \mathbf{X}_l^*$ and column index corresponding to point $x' \in \mathbf{X}_l^*$.

Now let $k = \prod_{j=1}^d k_j$ be a d -dimensional TMK and $\mathbf{X}_1^* = \times_{j=1}^d \mathbf{X}_{l_j}^*$ be a sorted FG. Then, R_1^{-1} , with R_1 the Cholesky decomposition of $k(\mathbf{X}_1^*, \mathbf{X}_1^*)$ can be directly calculated as

$$R_1^{-1} = \bigotimes_{j=1}^d R_{l_j}^{-1}, \quad (15)$$

where \bigotimes denotes the Kronecker product between matrices and $R_{l_j}^{-1}$ is the inverse Cholesky decomposition yielded by Algorithm 1 with input k_j and $\mathbf{X}_{l_j}^*$.

Let $R_{\mathbf{X}_1^*, \mathbf{X}_1^*}$ represent a sub-matrix of R consisting of entries $R_{\mathbf{x}, \mathbf{y}}$, $\mathbf{x}, \mathbf{y} \in \mathbf{X}_1^* \subset \mathbf{X}_l^{\text{SG}}$. Now we can present the algorithm of constructing R_l^{-1}

We will prove the correctness of Algorithm 1 and Algorithm 2 in later sections.

C Discussion on Algorithm 1

Before presenting the essential idea of Algorithm 1 in Appendix B, we first need to prove the following lemma and theorem.

Algorithm 1: Computing R^{-1} for Markov kernel k and point set \mathbf{X}_l^*

Input : Markov kernel k , level- l dyadic points \mathbf{X}_l^*

Output : R^{-1}

```

1 Initialize  $R^{-1} \leftarrow \mathbf{0} \in \mathbb{R}^{(2^l-1) \times (2^l-1)}$ ,  $\mathbf{N} = \{-\infty, \infty\}$ , define  $k(\pm\infty, x) = 0, \forall x$ 
2 for  $\ell \leftarrow 1$  to  $l$  do
3   for  $i \in \rho(\ell)$  do
4     search the closest left neighbor  $x_{left}$  and right neighbor  $x_{right}$  of  $x_{\ell,i}$  in  $\mathbf{N}$ 
5     Solve  $c_1, c_2$ , and  $c_3$  for the following system:
        
$$c_1 k(x_{left}, x_{left}) + c_2 k(x_{\ell,i}, x_{left}) + c_3 k(x_{right}, x_{left}) = 0,$$


$$c_1 k(x_{left}, x_{right}) + c_2 k(x_{\ell,i}, x_{right}) + c_3 k(x_{right}, x_{right}) = 0, \quad (14)$$


$$\mathbb{E}[(c_1 \mathcal{G}(x_{left}) + c_2 \mathcal{G}(x_{\ell,i}) + c_3 \mathcal{G}(x_{right}))^2] = 1$$

6     If  $x_{left} \neq -\infty$ ,  $[R^{-1}]_{x_{left}, x_{\ell,i}} = c_1$ 
7     If  $x_{right} \neq \infty$ ,  $[R^{-1}]_{x_{right}, x_{\ell,i}} = c_3$ 
8     Let  $[R^{-1}]_{x_{\ell,i}, x_{\ell,i}} = c_2$ ,  $x_{\ell,i} \rightarrow \mathbf{N}$ 
9   end
10 end
11 Return  $R^{-1}$ 

```

Lemma 2. Let k be a TMK defined on interval U and \mathcal{G} be the GP generated by k . For any $x < y < z$ in U , suppose c_1, c_2, c_3 satisfies the following conditions:

$$c_1 k(x, x) + c_2 k(y, x) + c_3 k(z, x) = 0,$$

$$c_1 k(x, z) + c_2 k(y, z) + c_3 k(z, z) = 0,$$

$$\mathbb{E}[(c_1 \mathcal{G}(x) + c_2 \mathcal{G}(y) + c_3 \mathcal{G}(z))^2] = 1.$$

Then function $\phi(\cdot) = c_1 k(\cdot, x) + c_2 k(\cdot, y) + c_3 k(\cdot, z)$ is compactly supported on $[x, z]$ and $\langle \phi, \phi \rangle_k = 1$ where $\langle \cdot, \cdot \rangle_k$ is the inner product generated by k .

Proof. From the definition of TMK in Lemma 1 in the main paper, the first two conditions

Algorithm 2: Computing R_l^{-1} for TMK k and level- l SG \mathbf{X}_l^{SG}

Input : TMK k , level- l SG \mathbf{X}_l^{SG}

Output : R_l^{-1}

```

1 Initialize  $R^{-1} \leftarrow \mathbf{0} \in \mathbb{R}^{m_l \times m_l}$ 
2 for all  $\mathbf{l} \in \mathbb{N}^d$  with  $l \leq |\mathbf{l}| \leq l + d - 1$  do
3   | Compute  $R_1^{-1}$  associated to  $(k, \mathbf{X}_1^*)$  via Algorithm 1 and (15)
4   | Update  $R_l^{-1}$  via
      | 
$$[R_l^{-1}]_{\mathbf{X}_1^*, \mathbf{X}_1^*} \leftarrow [R_l^{-1}]_{\mathbf{X}_1^*, \mathbf{X}_1^*} + (-1)^{l+d-1-|\mathbf{l}|} \binom{d-1}{l+d-1-|\mathbf{l}|} R_1^{-1} \quad (16)$$

5 end
6 Return  $R_l^{-1}$ 

```

can be written as

$$\begin{aligned}
p(x)(c_1q(x) + c_2q(y) + c_3q(z)) &= 0 \Rightarrow c_1q(x) + c_2q(y) + c_3q(z) = 0 \\
q(z)(c_1p(x) + c_2p(y) + c_3p(z)) &= 0 \Rightarrow c_1p(x) + c_2p(y) + c_3p(z) = 0.
\end{aligned}$$

So for any $s < x$

$$\begin{aligned}
\phi(s) &= c_1p(x \wedge s)q(x \vee s) + c_2p(y \wedge s)q(y \vee s) + c_3p(z \wedge s)q(z \vee s) \\
&= p(s)(c_1q(x) + c_2q(y) + c_3q(z)) \\
&= 0,
\end{aligned}$$

and for any $s > z$

$$\phi(s) = q(s)(c_1p(x) + c_2p(y) + c_3p(z)) = 0.$$

This proves that the support of ϕ is $[x, z]$.

Let \mathbf{C}^T denote vector $[c_1, c_2, c_3]$, \mathbf{G}^T denote vector $[\mathcal{G}(x), \mathcal{G}(y), \mathcal{G}(z)]$, $\boldsymbol{\gamma}^T$ denote vector $[k(\cdot, x), k(\cdot, y), k(\cdot, z)]$ and \mathbf{K} denote the covariance matrix on x, y, z . Then the third condition reads

$$\mathbb{E}[\mathbf{C}^T \mathbf{G} \mathbf{G}^T \mathbf{C}] = \mathbf{C}^T \mathbf{K} \mathbf{C} = 1.$$

Therefore, we have

$$\langle \phi, \phi \rangle_k = \langle \mathbf{C}^T \boldsymbol{\gamma}, \boldsymbol{\gamma}^T \mathbf{C} \rangle_k = \mathbf{C}^T \mathbf{K} \mathbf{C} = 1.$$

□

We can notice that equation (14) in Algorithm 1 is exactly the three conditions listed in Lemma 2. The purpose of Algorithm 1 is, in fact, generate compactly supported orthonormal basis functions in the reproducing kernel Hilbert space (Hastie et al., 2009) generated by k as we show in the following theorem:

Theorem 3. *The hierarchical features*

$$\phi = R^{-1}k(\mathbf{X}_l^*, \cdot) = [\phi_{\ell,i}]_{x_{\ell,i} \in \mathbf{X}_l^*}$$

where R^{-1} generated by Algorithm 1 are orthonormal under inner product $\langle \cdot, \cdot \rangle_k$:

$$\langle \phi_{\ell,i}, \phi_{\ell',i'} \rangle_k = \mathbf{1}_{\{(\ell,i)=(\ell',i')\}}.$$

Proof. The theorem is a consequence of the way we sort the dyadic point set \mathbf{X}_l^* and Lemma 2. Remind that \mathbf{X}_l^* has the following multi-resolution structure:

$$\mathbf{X}_l^* = \bigcup_{\ell \leq l} \mathbf{D}_\ell = \bigcup_{\ell \leq l} \{i2^{-\ell} : i \in \boldsymbol{\rho}(\ell)\} = \bigcup_{\ell \leq l} \{x_{\ell,i} : i \in \boldsymbol{\rho}(\ell)\}.$$

We first prove the following claim:

1. Supports of functions $\{\phi_{\ell,i} : i \in \boldsymbol{\rho}(\ell)\}$ are mutually disjoint for any fixed ℓ .

In Algorithm 1, for any pair of points $x_{\ell,i}$ and $x_{\ell',i'}$ with $\ell > \ell'$, $x_{\ell',i'}$ must be processed ahead of $x_{\ell,i}$ because the outer for loop will run through all the points in $\mathbf{D}_{\ell'}$ before processing any point in \mathbf{D}_ℓ . Moreover, the left and right neighbors of any $x_{\ell,i}$ in the iteration for processing $x_{\ell,i}$ must be in $\mathbf{D}_{\ell'}$ and $\mathbf{D}_{\ell''}$ for some $\ell', \ell'' < \ell$.

In iteration (ℓ, i) , Lemma 2 tells that the support of $\phi_{\ell,i}$ is $[x_{left}, x_{right}]$ because

$$\phi_{\ell,i} = c_1 k(\cdot, x_{left}) + c_2 k(\cdot, x_{\ell,i}) + c_3 k(\cdot, x_{right})$$

where c_1, c_2, c_3 solve equation (14) in the iteration for processing $x_{\ell,i}$. When the outer loop is in the ℓ iteration, all points in $\mathbf{X}_{\ell-1}^*$ have already been added to \mathbf{N} . Remind that if we

sort points in $\mathbf{X}_{\ell-1}^*$ in increasing order, then $\mathbf{X}_{\ell-1}^* = \{2^{-(\ell-1)}, 2 \cdot 2^{-(\ell-1)}, \dots, 1 - 2^{-(\ell-1)}\}$.

So we have the following relation regarding the distance between $x_{\ell,i} = i2^{-\ell}$ and $\mathbf{X}_{\ell-1}^*$:

$$\{i2^{-\ell} - 2^{-\ell}, i2^{-\ell} + 2^{-\ell}\} = \arg \min_{x \in \mathbf{X}_{\ell-1}^*} |x - x_{\ell,i}| = \arg \min_{x \in \mathbf{X}_{\ell-1}^*} |x - i2^{-\ell}|.$$

On the other hand, for any other point in \mathbf{D}_ℓ , we have:

$$\min_{x_{\ell,i'} \in \mathbf{D}_\ell} |x_{\ell,i} - x_{\ell,i'}| = \min_{i' \in \rho(\ell)} |i2^{-\ell} - i'2^{-\ell}| = 2 \cdot 2^{-\ell}.$$

So both x_{left} and x_{right} are must be from $\mathbf{X}_{\ell-1}^*$ such that

$$x_{left} = i2^{-\ell} - 2^{-\ell}, \quad x_{right} = i2^{-\ell} + 2^{-\ell}.$$

Therefore, the supports of hierarchical features $\{\phi_{\ell,i} : i \in \rho(\ell)\}$ are

$$\{[i2^{-\ell} - 2^{-\ell}, i2^{-\ell} + 2^{-\ell}] : i = 1, 3, \dots, 2^\ell - 1\}$$

and they are mutually disjoint. We finish the proof of claim 1.

Disjoint supports of hierarchical features with the same index ℓ indicates that they are also mutually orthogonal under $\langle \cdot, \cdot \rangle_k$.

We now prove $\phi_{\ell',i'}$ and $\phi_{\ell,i}$ are also orthogonal for any $\ell' < \ell$. Without loss of generality, we can assume that $x_{\ell,i} < x_{\ell',i'}$. As a direct consequence of the fact that support of $\phi_{\ell,i}$ is $[x_{\ell,i} - 2^{-\ell}, x_{\ell,i} + 2^{-\ell}]$ and support of $\phi_{\ell',i'}$ is $[x_{\ell',i'} - 2^{-\ell'}, x_{\ell',i'} + 2^{-\ell'}]$, we have the following claim:

2. For any $x_{\ell,i} < x_{\ell',i'}$ with $\ell' < \ell$ and $i \in \rho(\ell)$, $i' \in \rho(\ell')$, there are only two possible cases regarding the supports of $\phi_{\ell',i'}$ and $\phi_{\ell,i}$:

(a) $[x_{\ell,i} - 2^{-\ell}, x_{\ell,i} + 2^{-\ell}]$ and $[x_{\ell',i'} - 2^{-\ell'}, x_{\ell',i'} + 2^{-\ell'}]$ are disjoint;

(b) $[x_{\ell,i} - 2^{-\ell}, x_{\ell,i} + 2^{-\ell}] \subset [x_{\ell',i'} - 2^{-\ell'}, x_{\ell',i'} + 2^{-\ell'}]$.

For case **(a)** supports of $\phi_{\ell',i'}$ and $\phi_{\ell,i}$ are disjoint, the inner product $\langle \phi_{\ell',i'}, \phi_{\ell,i} \rangle_k = 0$.

To analyze case **(b)**, we first use the following identity:

$$\langle \phi_{\ell',i'}, \phi_{\ell,i} \rangle_k = \mathbf{C}_{\ell',i'}^T k(\mathbf{X}_{\ell',i'}, \mathbf{X}_{\ell,i}) \mathbf{C}_{\ell,i}.$$

In the above equation, point set $\mathbf{X}_{\ell,i}$ consists of the left and right neighbors of $x_{\ell,i}$, and $x_{\ell,i}$ itself. $\mathbf{C}_{\ell,i} = [c_1, c_2, c_3]^T$ where c_1, c_2, c_3 are the solution of equation (14) in the iteration for process $\phi_{\ell,i}$. $\mathbf{X}_{\ell',i'}$ and $\mathbf{C}_{\ell',i'}$ are defined in the same manner.

Because $[x_{\ell,i} - 2^{-\ell}, x_{\ell,i} + 2^{-\ell}] \subset [x_{\ell',i'} - 2^{-\ell'}, x_{\ell',i'}]$, and TMK $k(x, y) = p(x \wedge y)q(x \vee y)$, we have:

$$\begin{aligned}
& \langle \phi_{\ell,i}, \phi_{\ell',i'} \rangle_k \\
&= \mathbf{C}_{\ell,i}^T k(\mathbf{X}_{\ell,i}, \mathbf{X}_{\ell',i'}) \mathbf{C}_{\ell',i'} \\
&= \mathbf{C}_{\ell,i}^T \begin{bmatrix} p(x_{\ell',i'} - 2^{-\ell'})q(x_{\ell,i} - 2^{-\ell}) & p(x_{\ell,i} - 2^{-\ell})q(x_{\ell',i'}) & p(x_{\ell,i} - 2^{-\ell})q(x_{\ell',i'} + 2^{-\ell'}) \\ p(x_{\ell',i'} - 2^{-\ell'})q(x_{\ell,i}) & p(x_{\ell,i})q(x_{\ell',i'}) & p(x_{\ell,i})q(x_{\ell',i'} + 2^{-\ell'}) \\ p(x_{\ell',i'} - 2^{-\ell'})q(x_{\ell,i} + 2^{-\ell}) & p(x_{\ell,i} + 2^{-\ell})q(x_{\ell',i'}) & p(x_{\ell,i} + 2^{-\ell})q(x_{\ell',i'} + 2^{-\ell'}) \end{bmatrix} \mathbf{C}_{\ell',i'} \\
&= 0
\end{aligned}$$

where the last line can be derived directly from the first two conditions in Lemma 2 imposed on $\mathbf{C}_{\ell,i}$ and $\mathbf{C}_{\ell',i'}$. □

Lemma 2 and Theorem 3 show that the matrix R generated by Algorithm 1 is indeed the Cholesky decomposition of the covariance matrix:

Corollary 1. R^{-1} is a upper triangular matrix and $R^{-T}k(\mathbf{X}_l^*, \mathbf{X}_l^*)R^{-1} = \mathbf{I}$.

Proof. From our analysis in Theorem 3, we know that in the iteration for processing any $x_{\ell,i}$, x_{left} and x_{right} are from $\mathbf{D}_{\ell'}$ and $\mathbf{D}_{\ell''}$ with some $\ell', \ell'' < \ell$. According to how we sort \mathbf{X}_l^* , entries $[R^{-1}]_{x_{left}, x_{\ell,i}}$, $[R^{-1}]_{x_{\ell,i}, x_{\ell,i}}$, and $[R^{-1}]_{x_{right}, x_{\ell,i}}$ are in the upper triangular part of R^{-1} . In Algorithm 1, operation in iteration for processing $x_{\ell,i}$ is assigning values to three entries of R^{-1} , namely, $[R^{-1}]_{x_{left}, x_{\ell,i}}$, $[R^{-1}]_{x_{\ell,i}, x_{\ell,i}}$, and $[R^{-1}]_{x_{right}, x_{\ell,i}}$ and let any other value on column $[R^{-1}]_{:, x_{\ell,i}}$ equal 0. Therefore, the returned matrix R^{-1} is a upper triangular matrix.

From Theorem 3, we know that $\phi = k(\cdot, \mathbf{X}_l^*)R^{-1}$ are orthonormal basis functions under $\langle \cdot, \cdot \rangle_k$. Therefore,

$$\mathbf{I} = \langle \phi, \phi \rangle_k = R^{-T}k(\mathbf{X}_l^*, \mathbf{X}_l^*)R^{-1}.$$

□

D Discussion on Algorithm 2

Algorithm 2 in our main paper is a special case of Plumlee (2014)[Algorithm 2]. Plumlee (2014)[Algorithm 2] is for computing the matrix $\mathbf{A}[k(\mathbf{X}_l^{\text{SG}}, \mathbf{X}_l^{\text{SG}})]^{-1}$ where k is any

kernel in tensor product form $k(\mathbf{x}, \mathbf{y}) = \prod_{j=1}^d k_j(x_j, y_j)$ and \mathbf{A} is any matrix. Plumlee (2014)[Algorithm 2] is written as follows:

Algorithm 3: Computing $\mathbf{A}[k(\mathbf{X}_l^{\text{SG}}, \mathbf{X}_l^{\text{SG}})]^{-1}$ for tensor kernel k , level- l SG \mathbf{X}_l^{SG} ,

and any matrix \mathbf{A}

Input : tensor kernel k , level- l SG \mathbf{X}_l^{SG} , matrix \mathbf{A}

Output : $\mathbf{A}[k(\mathbf{X}_l^{\text{SG}}, \mathbf{X}_l^{\text{SG}})]^{-1}$

1 Initialize $\tilde{\mathbf{A}} \leftarrow \mathbf{0} \in \mathbb{R}^{m_l \times m_l}$

2 **for** all $\mathbf{l} \in \mathbb{N}^d$ with $l \leq |\mathbf{l}| \leq l + d - 1$ **do**

3 Update $\tilde{\mathbf{A}}$ via

$$[\tilde{\mathbf{A}}]_{:, \mathbf{x}_1^*} \leftarrow [\tilde{\mathbf{A}}]_{:, \mathbf{x}_1^*} + (-1)^{l+d-1-|\mathbf{l}|} \binom{d-1}{l+d-1-|\mathbf{l}|} \mathbf{A}_{:, \mathbf{x}_l^*} [k(\mathbf{X}_1^*, \mathbf{X}_1^*)]^{-1} \quad (\text{P})$$

($[\tilde{\mathbf{A}}]_{:, \mathbf{x}_1^*}$ denotes the matrix with columns that correspond to \mathbf{X}_1^* and all rows of \mathbf{A})

4 **end**

5 Return $\tilde{\mathbf{A}}$

If we let the argument \mathbf{A} be $R_l^{-1}k(\mathbf{X}_l^{\text{SG}}, \mathbf{X}_l^{\text{SG}})$ then, obviously, the output $\tilde{\mathbf{A}}$ must be R_l^{-1} . To show that Algorithm 2 in our paper is correct, we only need to show that the matrix $\mathbf{A}_{:, \mathbf{x}_1^*} [k(\mathbf{X}_1^*, \mathbf{X}_1^*)]^{-1}$ in (P) equals to R_1^{-1} on rows associated to \mathbf{X}_1^* and equals 0 on any other row.

If $\mathbf{A} = R_l^{-1}k(\mathbf{X}_l^{\text{SG}}, \mathbf{X}_l^{\text{SG}})$, then $\mathbf{A}_{:, \mathbf{x}_1^*} [k(\mathbf{X}_1^*, \mathbf{X}_1^*)]^{-1} = R_l^{-1}k(\mathbf{X}_l^{\text{SG}}, \mathbf{X}_1^*) [k(\mathbf{X}_1^*, \mathbf{X}_1^*)]^{-1}$. From the definition of hierarchical features (9), we have

$$\mathbf{A}_{:, \mathbf{x}_1^*} [k(\mathbf{X}_1^*, \mathbf{X}_1^*)]^{-1} = R_l^{-1}k(\mathbf{X}_l^{\text{SG}}, \mathbf{X}_1^*) [k(\mathbf{X}_1^*, \mathbf{X}_1^*)]^{-1} = \phi(\mathbf{X}_1^*) [k(\mathbf{X}_1^*, \mathbf{X}_1^*)]^{-1}.$$

Based on the this identity, we can use the following theorem to immediately get the result:

Theorem 4. $\phi(\mathbf{X}_1^*)$ equals $R_1^{-1}k(\mathbf{X}_1^*, \mathbf{X}_1^*)$ on rows associated to \mathbf{X}_1^* and equals 0 on any other row.

Proof. Remind that a level- l sparse grid is defined as $\mathbf{X}_l^{\text{SG}} = \{\mathbf{x}_{\mathbf{l}, \mathbf{i}} : |\mathbf{l}| \leq l, \mathbf{i} \in \boldsymbol{\rho}(\mathbf{l})\}$, we can label hierarchical feature by its associated design point $\mathbf{x}_{\mathbf{l}, \mathbf{i}}$ in the sparse grid \mathbf{X}_l^{SG} :

$[\phi_{\mathbf{V},\mathbf{i}}]_{\mathbf{x}_{\mathbf{V}},\mathbf{i} \in \mathbf{X}_l^{\text{SG}}}$. Ding and Zhang (2020)[Lemma EC.1] states that

$$\phi_{\mathbf{V},\mathbf{i}} = \prod_{j=1}^d \phi_{\ell'_j, i_j}$$

where, for $j = 1, \dots, d$, $\phi_{\ell'_j, i_j}$ is the one-dimensional hierarchical feature associated to point $x_{\ell'_j, i_j}$ in one-dimensional set $\mathbf{D}_{\ell'_j}$ as we defined in Lemma 2 and Theorem 3.

Similarly, we can use Kronecker product technique to derive that

$$R_1^{-1}k(\mathbf{X}_1^*, \cdot) = \left[\bigotimes_{j=1}^d R_{l_j}^{-1} \right] \left[\bigotimes_{j=1}^d k_j(\mathbf{X}_{\ell_j}^*, \mathbf{X}_{\ell_j}^*) \right] = \bigotimes_{j=1}^d [\phi_{\ell'_j, i_j}]_{x_{\ell'_j, i_j} \in \mathbf{X}_{\ell_j}^*} = [\phi_{\ell', \mathbf{i}}]_{\mathbf{x}_{\ell', \mathbf{i}} \in \mathbf{X}_1^*}.$$

We can immediately see that $[\phi_{\ell', \mathbf{i}}]_{\mathbf{x}_{\ell', \mathbf{i}} \in \mathbf{X}_1^*}$ is a sub-vector of $[\phi_{\mathbf{V}, \mathbf{i}}]_{\mathbf{x}_{\mathbf{V}}, \mathbf{i} \in \mathbf{X}_l^{\text{SG}}}$ with rows associated to \mathbf{X}_1^* . As a result, it is obvious that $[\phi_{\ell', \mathbf{i}}(\mathbf{X}_1^*)]_{\mathbf{x}_{\ell', \mathbf{i}} \in \mathbf{X}_1^*}$ equals $[\phi_{\mathbf{V}, \mathbf{i}}(\mathbf{X}_1^*)]_{\mathbf{x}_{\mathbf{V}}, \mathbf{i} \in \mathbf{X}_l^{\text{SG}}}$ on rows associated to \mathbf{X}_1^* because these two vectors of functions have same entries of functions on these rows.

Let $\mathbf{D} = \mathbf{X}_l^{\text{SG}} - \mathbf{X}_1^*$ denote the difference set. The only thing left is to prove $[\phi_{\mathbf{V}, \mathbf{i}}(\mathbf{X}_1^*)]_{\mathbf{x}_{\mathbf{V}}, \mathbf{i} \in \mathbf{D}}$ equals zero. For any point $\mathbf{x}_{\mathbf{V}}, \mathbf{i} \in \mathbf{D}$, there must be some dimension j such that $\ell'_j > \ell_j$ for $\mathbf{x}_{\mathbf{V}}, \mathbf{i} \in \mathbf{X}_1^*$ otherwise. From our discussion in Theorem 3, we know that the support of $\phi_{\ell'_j, i_j}$ is $[i_j 2^{-\ell'} - 2^{-\ell'}, i_j 2^{-\ell'} + 2^{-\ell'}]$ where $i_j \in \boldsymbol{\rho}(\ell'_j)$ is odd. As a result, for any point $\mathbf{x}_{\mathbf{V}}, \mathbf{i}'' \in \mathbf{X}_1^*$, its j^{th} entry $x_{\ell'_j, i_j''}$ must satisfy $\ell_j'' < \ell'_j$ and $i_j'' \in \boldsymbol{\rho}(\ell_j'')$ is odd. Therefore, it is straightforward to derive that

$$x_{\ell'_j, i_j''} = i_j'' 2^{-\ell''} \notin (i_j 2^{-\ell'} - 2^{-\ell'}, i_j 2^{-\ell'} + 2^{-\ell'}) \quad \text{for any } i_j \in \boldsymbol{\rho}(\ell'_j) \text{ odd.}$$

This leads to $\phi_{\ell'_j, i_j}(x_{\ell'_j, i_j''}) = 0$ and, hence, $\phi_{\mathbf{V}, \mathbf{i}}(\mathbf{x}_{\ell'', \mathbf{i}}) = 0$. \square

E Proof of Theorem 1:

Proof. We first count the number of non-zero entries on R_l^{-1} . From Appendix B, Algorithm 2, we can see that R_l^{-1} is the summation of matrices of the form $R_1^{-1} = \bigotimes_{j=1}^d R_{l_j}^{-1}$. So we first count the number of non-zero entries on these matrices. Because, $R_{l_j}^{-1}$ is a $(2^{l_j} - 1)$ -by- $(2^{l_j} - 1)$ sparse matrix with $\mathcal{O}(2^{l_j})$ non-zero entries as shown in Appendix B-Algorithm 1, the total number of non-zero entries on R_1^{-1} is $\mathcal{O}(2^{|\mathbf{l}|})$. Then the total number of non-zero entries of R_l^{-1} in Appendix B, Algorithm 2 should be bounded by the following sum:

$$\sum_{l \leq |\mathbf{l}| \leq l+d-1} \mathcal{O}(2^{|\mathbf{l}|}) = \mathcal{O}\left(\sum_{\ell=0}^{l-1} 2^\ell \binom{\ell + d - 1}{d - 1}\right) = \mathcal{O}(|\mathbf{X}_l^{\text{SG}}|) = \mathcal{O}(m_l),$$

where the last equality is exactly equation (13).

We now count the time complexity of Appendix B, Algorithm 2. In each iteration, the time complexity for constructing R_1^{-1} is

$$\left(\sum_{j=1}^d \mathcal{O}(2^{l_j})\right) + \mathcal{O}(2^{|\mathbf{l}|}) = \mathcal{O}(2^{|\mathbf{l}|}),$$

where the first term on the left-hand side is the time complexity for constructing each component $R_{l_j}^{-1}$, $j = 1, \dots, d$, in the Kronecker product and the second term is the time complexity for computing the Kronecker product of upper triangular matrices.

Similar to our counting for its non-zero entries, the total time complexity is then

$$\mathcal{O}\left(\sum_{l \leq |\mathbf{l}| \leq l+d-1} 2^{|\mathbf{l}|}\right) = \mathcal{O}(m_l).$$

□

F Proof of Theorem 2:

Proof. To prove this theorem, we need two more algorithms for computing hierarchical features. The first algorithm is developed from Appendix B-Algorithm 1:

We first count the number of non-zero entries on the output of Algorithm 4. Given any x^* , we first fix a ℓ in the outer for-loop. From Lemma 2, we can derive that the only non-zero $[\phi]_{x_{\ell,i}}$ is the (ℓ, i) satisfying the requirement $x_{left} < x^* < x_{right}$.

Because of the way we sort $\mathbf{X}_l^* = [\mathbf{D}_1 \mathbf{D}_2 \dots \mathbf{D}_l]$, all the points $\{x_{\ell,i}, i \in \boldsymbol{\rho}(\ell)\}$ in the inner for-loop are in \mathbf{D}_ℓ and none of their closet neighbor is in \mathbf{D}_ℓ . As a result, for any fixed ℓ , there is only one (ℓ, i) satisfies $x_{left} < x^* < x_{right}$ in the inner-loop and, hence, there is only one non-zero entry is added to ϕ in Algorithm 4 in each other iteration. This shows that the number of non-zero on the output of Algorithm 4 is l .

We then propose an algorithm to compute $\phi(\mathbf{x}^*) = R_l^{-T} k(\mathbf{X}_l^{\text{SG}}, \mathbf{x}^*)$ as shown in Algorithm 5. Algorithm 5 is a simple extension of Appendix B-Algorithm 2. Based on this algorithm, we can estimate the number of non-zero entries on $\phi(\mathbf{x}^*)$.

We first estimate the number of non-zero entries for $\phi_1(\mathbf{x}^*)$ in each iteration. Because the number of non-zero entries on each $[R^T]_{l_j}^{-1} k_j(\mathbf{X}_{l_j}^*, x_j^*)$ is l_j , the total number of non-zero entries on tensor $\phi_1(\mathbf{x}^*)$ is $\mathcal{O}(\prod_{j=1}^d l_j)$.

Algorithm 4: Computing $[R^T]^{-1}k(\mathbf{X}_1^*, x^*)$ for Markov kernel k and point set \mathbf{X}_l^*

Input : Markov kernel k , level- l dyadic points \mathbf{X}_l^* , and input x^*

Output : $[R^T]^{-1}k(\mathbf{X}_1^*, x^*)$

```

1 Initialize  $\phi \leftarrow \mathbf{0} \in \mathbb{R}^{(2^l-1)}$ ,  $\mathbf{N} = \{-\infty, \infty\}$ , define  $k(\pm\infty, x) = 0, \forall x$ 
2 for  $\ell \leftarrow 1$  to  $l$  do
3   for  $i \in \rho(\ell)$  do
4     search the closest left neighbor  $x_{left}$  and right neighbor  $x_{right}$  of  $x_{\ell,i}$  in  $\mathbf{N}$ 
5     Solve  $c_1, c_2$ , and  $c_3$  associated to  $x_{left}, x_{\ell,i}$ , and  $x_{right}$  in equation (14) in
       Appendix B
6     Update  $[\phi]_{x_{\ell,i}}$  via
           
$$[\phi]_{x_{\ell,i}} = c_1 k(x_{left}, x^*) + c_2 k(x_{\ell,i}, x^*) + c_3 k(x_{right}, x^*) \quad (\text{s.1})$$

7      $x_{\ell,i} \rightarrow \mathbf{N}$ 
8   end
9 end
10 Return  $[R^T]^{-1}k(\mathbf{X}_1^*, x^*) = \phi$ 

```

Because only a constant amount of entries are flipped from zero to non-zero in each iteration in Algorithm 5, the total number of non-zero entries of $\phi(\mathbf{x}^*)$ is

$$\mathcal{O}\left(\sum_{l \leq |\mathbf{l}| \leq l+d-1} \prod_{j=1}^d l_j\right) = \mathcal{O}\left(\sum_{\ell=0}^{l-1} \ell^d \binom{\ell+d-1}{d-1}\right) = \mathcal{O}(l^{2d-1}) = \mathcal{O}([\log m_l]^{2d-1}).$$

□

G Approximation Error of Hierarchical Expansion

Compared with the original DGP proposed in Damianou and Lawrence (2013), every output unit in a DTMGP is, in fact, the finite-rank hierarchical expansion of a tensor Markov GP given that output unit is linear combination of finitely many random hierarchical features. Therefore, we first analyze how well hierarchical expansion can approximate a tensor Markov GP. This leads to the following theorem:

Theorem 5. *Let \mathcal{G} be a TMGP with TMK k . Given any level- l SG \mathbf{X}_l^{SG} , we have the*

Algorithm 5: Computing $\phi(\mathbf{x}^*)$ for TMK k , level- l SG \mathbf{X}_l^{SG} and input \mathbf{x}^*

Input : TMK k , level- l SG \mathbf{X}_l^{SG} , input \mathbf{x}^*

Output : $\phi(\mathbf{x}^*)$

1 Initialize $\phi(\mathbf{x}^*) \leftarrow \mathbf{0} \in \mathbb{R}^{m_l}$

2 **for** all $\mathbf{l} \in \mathbb{N}^d$ with $l \leq |\mathbf{l}| \leq l + d - 1$ **do**

3 Compute $\{[R^T]_{l_j}^{-1} k_j(\mathbf{X}_{l_j}^*, x_j^*)\}_{j=1}^d$ via Algorithm 4

4 Compute $\phi_{\mathbf{l}}(\mathbf{x}^*) = [R^T]_{\mathbf{l}}^{-1} k(\mathbf{X}_{\mathbf{l}}^*, \mathbf{x}^*)$ via

$$\phi_{\mathbf{l}}(\mathbf{x}^*) = \bigotimes_{j=1}^d [R^T]_{l_j}^{-1} k_j(\mathbf{X}_{l_j}^*, x_j^*). \quad (\text{s.2})$$

5 Update $\phi(\mathbf{x}^*)$ via

$$[\phi(\mathbf{x}^*)]_{\mathbf{x}_1^*} \leftarrow [\phi(\mathbf{x}^*)]_{\mathbf{x}_1^*} + (-1)^{l+d-1-|\mathbf{l}|} \binom{d-1}{l+d-1-|\mathbf{l}|} \phi_{\mathbf{l}}(\mathbf{x}^*) \quad (\text{s.3})$$

6 **end**

7 **Return** $\phi(\mathbf{x}^*)$

following L^2 distance between \mathcal{G} and its hierarchical expansion with inducing variables \mathbf{X}_l^{SG}

$$\max_{\mathbf{x} \in (0,1)^D} \mathbb{E}[|\mathcal{G}(\mathbf{x}) - \phi^T(\mathbf{x})\mathbf{Z}|^2] = \mathcal{O}\left(\frac{l^{2d-2}}{2^l}\right) = \mathcal{O}\left(\frac{[\log m_l]^{2d-2}}{m_l}\right),$$

where $\mathbf{Z} = [R_l^T]^{-1} \mathcal{G}(\mathbf{X}_l^{\text{SG}})$ is a vector of i.i.d. standard Gaussian random variables and $\mathcal{G}(\mathbf{X}_l^{\text{SG}})$ are samples of \mathcal{G} on \mathbf{X}_l^{SG} .

Proof of Theorem 5. We prove by induction on dimension D . For the base case $D = 1$, notice that sparse grid \mathbf{X}_l^{SG} is then reduced to a dyadic grid $\{2^{-l}, 2 \cdot 2^{-l}, \dots, 1 - 2^{-l}\}$ and TMGP \mathcal{G} is a Markov process. From the Markov property of \mathcal{G} , we have

$$\begin{aligned} \max_{x \in (0,1)} \mathbb{E}[|\mathcal{G}(x) - \phi^T(x)\mathbf{Z}|^2] &= \max_{x \in (0,1)} \mathbb{E}[|\mathcal{G}(x) - k(x, \mathbf{X}_l^{\text{SG}}) \mathbf{K}^{-1} \mathcal{G}(\mathbf{X}_l^{\text{SG}})|^2] \\ &= \max_{i=1, \dots, 2^l} \max_{x \in ((i-1)2^{-l}, i2^{-l})} \mathbb{E}[|\mathcal{G}(x) - k(x, \mathbf{X}_i) \mathbf{K}_i^{-1} \mathcal{G}(\mathbf{X}_i)|^2] \end{aligned}$$

where $\mathbf{K} = k(\mathbf{X}_l^{\text{SG}}, \mathbf{X}_l^{\text{SG}})$, $\mathbf{X}_i = \{(i-1)2^{-l}, i2^{-l}\}$ for $1 < i < 2^l$, $\mathbf{X}_1 = \{2^{-l}\}$, $\mathbf{X}_{2^l} = \{1 - 2^{-l}\}$, and $\mathbf{K}_i = k(\mathbf{X}_i, \mathbf{X}_i)$. The last line of the above equations is from the following reasoning. $\mathcal{G}(x) - k(x, \mathbf{X}_l^{\text{SG}}) \mathbf{K}^{-1} \mathcal{G}(\mathbf{X}_l^{\text{SG}})$ can be treated as a Markov GP which equals 0 on \mathbf{X}_l^{SG} and, therefore, the distribution of $\mathcal{G}(x) - k(x, \mathbf{X}_l^{\text{SG}}) \mathbf{K}^{-1} \mathcal{G}(\mathbf{X}_l^{\text{SG}})$ is independent

of $\mathcal{G}(y) - k(y, \mathbf{X}_l^{\text{SG}}) \mathbf{K}^{-1} \mathcal{G}(\mathbf{X}_l^{\text{SG}})$ for any pair of x, y not sharing the same left and right neighboring points in \mathbf{X}_l^{SG} .

Now for any i and $x \in ((i-1)2^{-l}, i2^{-l})$, the posterior $M_i(x) := \mathcal{G}(x) - k(x, \mathbf{X}_i) \mathbf{K}_i^{-1} \mathcal{G}(\mathbf{X}_i)$ can be treated again as a Markov GP with fixed boundary at x_{i-1} and x_i . Because M_i is a Markov GP defined on interval of length 2^{-l} with fixed boundary condition, it is straightforward to derive that $\max_x \mathbb{E}[|M_i(x)|^2] = \mathcal{O}(2^{-l})$. This holds for any i so we can get when dimension $D = 1$,

$$\max_{x \in (0,1)} \mathbb{E}[|\mathcal{G}(x) - \phi^T(x) \mathbf{Z}|^2] = \max_{i=1, \dots, 2^l} \max_{x \in \mathcal{I}_i} \mathbb{E}[|\mathcal{G}(x) - k(x, \mathbf{X}_i) \mathbf{K}_i^{-1} \mathcal{G}(\mathbf{X}_i)|^2] = \mathcal{O}(2^{-l}).$$

where \mathcal{I}_i denote the interval $((i-1)2^{-l}, i2^{-l})$.

Now suppose our theorem holds for $D = d-1$. We now prove the case $D = d$. Let $\prod_{j=1}^d k_j$ denote TMK $k(\mathbf{x}, \mathbf{x})$. For any \mathbf{x} , the L^2 distance has the following identity

$$\begin{aligned} & \mathbb{E}[|\mathcal{G}(\mathbf{x}) - \phi^T(\mathbf{x}) \mathbf{Z}|^2] \\ &= \mathbb{E}[|\mathcal{G}(\mathbf{x}) - k(\mathbf{x}, \mathbf{X}_l^{\text{SG}}) \mathbf{K}^{-1} \mathcal{G}(\mathbf{X}_l^{\text{SG}})|^2] \\ &= k(\mathbf{x}, \mathbf{x}) - k(\mathbf{x}, \mathbf{X}_l^{\text{SG}}) \mathbf{K}^{-1} k(\mathbf{X}_l^{\text{SG}}, \mathbf{x}) \\ &= \prod_{j=1}^d k_j - \phi^T(\mathbf{x}) \phi(\mathbf{x}). \end{aligned}$$

Let $\hat{k}_j^{(l)}$ denote $k_j(x, \mathbf{X}_{l_j}^*) [k_j(\mathbf{X}_{l_j}^*, \mathbf{X}_{l_j}^*)]^{-1} k(\mathbf{X}_{l_j}^*, x)$ where $\mathbf{X}_{l_j}^*$ is the dyadic point set defined in the proof of theorem 2. As a direct result of Algorithm 5, we have

$$\begin{aligned} & \phi^T(\mathbf{x}) \phi(\mathbf{x}) \\ &= \sum_{|\mathbf{l}|=l}^{l+d-1} (-1)^{l+d-1-|\mathbf{l}|} \binom{d-1}{l+d-1-|\mathbf{l}|} \phi_1^T(\mathbf{x}) \phi_1(\mathbf{x}) \\ &= \sum_{|\mathbf{l}|=l}^{l+d-1} (-1)^{l+d-1-|\mathbf{l}|} \binom{d-1}{l+d-1-|\mathbf{l}|} \left[\bigotimes_{j=1}^d [R^T]_{l_j}^{-1} k_j(\mathbf{X}_{l_j}^*, x_j^*) \right]^T \left[\bigotimes_{j=1}^d [R^T]_{l_j}^{-1} k_j(\mathbf{X}_{l_j}^*, x_j^*) \right] \\ &= \sum_{|\mathbf{l}|=l}^{l+d-1} (-1)^{l+d-1-|\mathbf{l}|} \binom{d-1}{l+d-1-|\mathbf{l}|} \prod_{j=1}^d \hat{k}_j^{(l_j)}. \end{aligned}$$

The last line of the above equations can be derive by induction on the following identity of Kronecker product:

$$[(\mathbf{M}_2 v_2) \otimes (\mathbf{M}_1 v_1)]^T [(\mathbf{M}_2 v_2) \otimes (\mathbf{M}_1 v_1)] = \left(v_2^T \mathbf{M}_2^T \mathbf{M}_2 v_2 \right) \left(v_1^T \mathbf{M}_1^T \mathbf{M}_1 v_1 \right)$$

where \mathbf{M}_i is any m -by- m matrix and v_i is any m -by-1 vector for $i = 1, 2$.

Let $\Delta_j^{(l)}$ denote $\hat{k}_j^{(l)} - \hat{k}_j^{(l-1)}$ and \mathbf{l}_{-d} denote the vector (l_1, \dots, l_{d-1}) . We have the following identity:

$$\begin{aligned}
& \sum_{|\mathbf{l}|=l}^{l+d-1} (-1)^{l+d-1-|\mathbf{l}|} \binom{d-1}{l+d-1-|\mathbf{l}|} \prod_{j=1}^d \hat{k}_j^{(l_j)} \\
&= \sum_{|\mathbf{l}| \leq l+d-1} \prod_{j=1}^d \Delta_j^{(l_j)} \\
&= \sum_{i=d}^{l+d-1} \sum_{|\mathbf{l}|=i} \prod_{j=1}^d \Delta_j^{(l_j)} \\
&= \sum_{i=d}^{l+d-1} \sum_{|\mathbf{l}_{-d}|=d-1}^{i-1} (\hat{k}_d^{(i-|\mathbf{l}_{-d}|)} - \hat{k}_d^{(i-1-|\mathbf{l}_{-d}|)}) \prod_{j=1}^{d-1} \Delta_j^{(l_j)} \\
&= \sum_{|\mathbf{l}_{-d}|=d-1}^{l+d-2} \hat{k}_d^{(l+d-1-|\mathbf{l}_{-d}|)} \prod_{j=1}^{d-1} \Delta_j^{(l_j)}.
\end{aligned}$$

where the last line is from telescoping sum. Hence, the L^2 distance becomes

$$\begin{aligned}
& \prod_{j=1}^d k_j - \sum_{|\mathbf{l}|=l}^{l+d-1} (-1)^{l+d-1-|\mathbf{l}|} \binom{d-1}{l+d-1-|\mathbf{l}|} \prod_{j=1}^d \hat{k}_j^{(l_j)} \\
&= \prod_{j=1}^d k_j - \sum_{|\mathbf{l}_{-d}|=d-1}^{l+d-2} \hat{k}_d^{(l+d-1-|\mathbf{l}_{-d}|)} \prod_{j=1}^{d-1} \Delta_j^{(l_j)} \\
&= k_d \left(\prod_{j=1}^{d-1} k_j - \sum_{|\mathbf{l}_{-d}|=d-1}^{l+d-2} \prod_{j=1}^{d-1} \Delta_j^{(l_j)} \right) + \sum_{|\mathbf{l}_{-d}|=d-1}^{l+d-2} (k_d - \hat{k}_d^{(l+d-1-|\mathbf{l}_{-d}|)}) \prod_{j=1}^{d-1} \Delta_j^{(l_j)} \\
&= \mathcal{O}\left(\frac{l^{2(d-2)}}{2^l}\right) + \mathcal{O}\left(\sum_{|\mathbf{l}_{-d}|=d-1}^{l+d-2} 2^{-l}\right) \tag{s.4}
\end{aligned}$$

where the last line is from our induction hypothesis. From direct calculation, we then get

$$\sum_{|\mathbf{l}_{-d}|=d-1}^{l+d-2} 2^{-l} = 2^{-l} \sum_{i=d-1}^{l+d-2} \binom{i-2}{d-2} = \mathcal{O}\left(\frac{l^{2(d-1)}}{2^l}\right). \tag{s.5}$$

Lemma 3.6 in Bungartz and Griebel (2004) stipulates that the sample size of \mathbf{X}_l^{SG} is given by

$$m_l = \left| \mathbf{X}_l^{\text{SG}} \right| = \sum_{\ell=0}^{l-1} 2^\ell \binom{\ell+d-1}{d-1} = 2^l \cdot \left(\frac{l^{d-1}}{(d-1)!} + \mathcal{O}(l^{d-2}) \right) = \mathcal{O}(2^l l^{d-1}). \tag{s.6}$$

Putting (s.4),(s.5),(s.6), we can get the final result:

$$\prod_{j=1}^d k_j - \sum_{|\mathbf{l}|=l}^{l+d-1} (-1)^{l+d-1-|\mathbf{l}|} \binom{d-1}{l+d-1-|\mathbf{l}|} \prod_{j=1}^d \hat{k}_j^{(l_j)} = \mathcal{O}\left(\frac{l^{2(d-1)}}{2^l}\right) = \mathcal{O}\left(\frac{[\log m_l]^{2d-2}}{m_l}\right).$$

□

H Approximation Error of DTMGP

The sparse property of hierarchical features in each layer yields efficient training and inference of DTMGP. Furthermore, hierarchical features are nearly the optimal choice of features in recovering the underlying TMGP as shown in Ding et al. (2020). The sparsity and optimality of $\{\phi^{(h)}\}_{h=1}^H$ leads to the following theorem regarding the approximation capacity of DTMGP:

Theorem 6. *Let $f^{(H)} : \mathbb{R}^{W^{(0)}} \rightarrow \mathbb{R}^{W^{(H)}}$ be a layer- H DGP such that layer h of $f^{(H)}$ consists of a $W^{(h)}$ -variate TMGP, for $h = 1, \dots, d$. Let DTMGP $\mathcal{T}^{(H)}$ be the hierarchical expansion of $f^{(H)}$ such that $\mathcal{T}^{(H)}$ uses $m^{(h)}$ hierarchical features to approximate the $W^{(h)}$ -variate TMGP in layer h of $f^{(H)}$. We then have the following L^2 distance between $\mathcal{T}^{(H)}$ and $f^{(H)}$:*

$$\begin{aligned} & \max_{\mathbf{x}} \left(\mathbb{E} [\|f^{(H)}(\mathbf{x}) - \mathcal{T}^{(H)}(\mathbf{x})\|^2] \right)^{\frac{1}{2}} \\ & \leq C \sum_{h=1}^H \left(\frac{W^{(h)} (\log m^{(h)})^{2W^{(h-1)}-2}}{m^{(h)}} \right)^{\frac{1}{2H-h+1}} \prod_{\gamma=h+1}^H \left(W^{(\gamma)} \right)^{\frac{1}{2H-\gamma+1}}, \end{aligned}$$

where C is some constant independent of $\{m^{(h)}\}_{h=1}^H$.

Proof of Theorem 6. Let $\mathcal{G}^{(h)}$ denote the TMGP in layer h of $f^{(H)}$ and let $\tilde{\mathcal{G}}^{(h)}$ denote the hierarchical expansion of $\mathcal{G}^{(h)}$. We prove the statement by induction in the number of layers H . When $H = 1$, the statement is obviously true because it is equivalent to Theorem 5.

Now suppose the statement holds for the case $H - 1$, then for H and any \mathbf{x} , we have

$$\begin{aligned}
& \left(\mathbb{E} [\|f^{(H)}(\mathbf{x}) - \mathcal{T}^{(H)}(\mathbf{x})\|^2] \right)^{\frac{1}{2}} \\
&= \left(\mathbb{E} [\|\mathcal{G}^{(H)} \circ f^{(H-1)}(\mathbf{x}) - \tilde{\mathcal{G}}^{(H)} \circ \mathcal{T}^{(H-1)}(\mathbf{x})\|^2] \right)^{\frac{1}{2}} \\
&= \left(\mathbb{E} [\|\mathcal{G}^{(H)} \circ f^{(H-1)}(\mathbf{x}) - \tilde{\mathcal{G}}^{(H)} \circ f^{(H-1)}(\mathbf{x}) + \tilde{\mathcal{G}}^{(H)} \circ f^{(H-1)}(\mathbf{x}) - \tilde{\mathcal{G}}^{(H)} \circ \mathcal{T}^{(H-1)}(\mathbf{x})\|^2] \right)^{\frac{1}{2}} \\
&\leq \left(\mathbb{E} [\|\mathcal{G}^{(H)} \circ f^{(H-1)}(\mathbf{x}) - \tilde{\mathcal{G}}^{(H)} \circ f^{(H-1)}(\mathbf{x})\|^2] \right)^{\frac{1}{2}} \tag{s.7}
\end{aligned}$$

$$+ \left(\mathbb{E} [\|\tilde{\mathcal{G}}^{(H)} \circ f^{(H-1)}(\mathbf{x}) - \tilde{\mathcal{G}}^{(H)} \circ \mathcal{T}^{(H-1)}(\mathbf{x})\|^2] \right)^{\frac{1}{2}}, \tag{s.8}$$

where the fourth line is from triangular inequality.

According to theorem 5, we can directly derive the following upper bound of (s.7)

$$\left(\mathbb{E} [\|\mathcal{G}^{(H)} \circ f^{(H-1)}(\mathbf{x}) - \tilde{\mathcal{G}}^{(H)} \circ f^{(H-1)}(\mathbf{x})\|^2] \right)^{\frac{1}{2}} \leq C \sqrt{\frac{W^{(H)}(\log m^{(H)})^{2W^{(H-1)}-2}}{m^{(H)}}}, \tag{s.9}$$

for some C independent of $m^{(H)}$ and $W^{(H)}$.

Now we estimate the upper bound of (s.8). Because hierarchical expansion is an induced approximation, it does not change the Hölder condition of the Gaussian process, we can have:

$$\mathbb{E} [\|\tilde{\mathcal{G}}^{(H)} \circ f^{(H-1)}(\mathbf{x}) - \tilde{\mathcal{G}}^{(H)} \circ \mathcal{T}^{(H-1)}(\mathbf{x})\|^2] \leq C' \mathbb{E} [\|\mathcal{G}^{(H)} \circ f^{(H-1)}(\mathbf{x}) - \mathcal{G}^{(H)} \circ \mathcal{T}^{(H-1)}(\mathbf{x})\|^2],$$

for some C' independent of $f^{(H-1)}$ and $\mathcal{T}^{(H-1)}$. Now we estimate the Hölder condition of \mathcal{G} along all dimensions of its input $\mathbf{f} = (f_1, \dots, f_{W^{(h-1)}})$:

$$\begin{aligned}
& \frac{\mathbb{E} [\|\mathcal{G}^{(H)}(\mathbf{f}) - \mathcal{G}^{(H)}(\mathbf{f} + h\mathbf{e}_j)\|^2]}{h} \\
&= W^{(H)} \frac{k(f_j, f_j) + k(f_j + h, f_j + h) - 2k(f_j, f_j + h)}{h} \\
&= W^{(H)} \frac{p(f_j)q(f_j) + p(f_j)q(f_j + h) - 2p(f_j)q(f_j + h)}{h} \\
&= C'' W^{(H)}, \quad \text{for } j = 1, \dots, W^{(h-1)}, \tag{s.10}
\end{aligned}$$

where C'' is some constant independent of \mathbf{f} , h is any small positive constant, \mathbf{e}_j is a zero vector with the j^{th} entry equals 1, k is the TMK of $\mathcal{G}^{(H)}$, and the third line is from definition of TMK k , the last line is from Lemma 1 in the main paper.

Then, we have the following estimate of (s.8):

$$\begin{aligned}
& \left(\mathbb{E} [\| \tilde{\mathcal{G}}^{(H)} \circ f^{(H-1)} - \tilde{\mathcal{G}}^{(H)} \circ \mathcal{T}^{(H-1)} \|^2] \right)^{\frac{1}{2}} \\
& \leq C''' \sqrt{W^{(H)} \left(\mathbb{E} \| f^{(H-1)} - \mathcal{T}^{(H-1)} \|^2 \right)^{\frac{1}{2}}} \\
& \leq C'''' \sqrt{W^{(H)} \sum_{h=1}^{H-1} \left(\frac{W^{(h)} (\log m^{(h)})^{2W^{(h-1)}-2}}{m^{(h)}} \right)^{\frac{1}{2^{H-h}}} \prod_{\gamma=h+1}^{H-1} \left(W^{(\gamma)} \right)^{\frac{1}{2^{H-\gamma}}}} \\
& \leq C'''' \sqrt{W^{(H)} \sum_{h=1}^{H-1} \sqrt{\left(\frac{W^{(h)} (\log m^{(h)})^{2W^{(h-1)}-2}}{m^{(h)}} \right)^{\frac{1}{2^{H-h}}} \prod_{\gamma=h+1}^{H-1} \left(W^{(\gamma)} \right)^{\frac{1}{2^{H-\gamma}}}}} \\
& = C'''' \sum_{h=1}^{H-1} \left(\frac{W^{(h)} (\log m^{(h)})^{2W^{(h-1)}-2}}{m^{(h)}} \right)^{\frac{1}{2^{H-h+1}}} \prod_{\gamma=h+1}^H \left(W^{(\gamma)} \right)^{\frac{1}{2^{H-\gamma+1}}}, \tag{s.11}
\end{aligned}$$

where C''' and C'''' are some number independent of $\{m^{(h)}\}_{h=1}^{H-1}$, the second line is from the Hölder condition (s.10), the third line is from the induction assumption.

Putting equations (s.9) and (s.11) together, we can have the final result. \square

From theorem (6), we can see that if a DTMGP is not tremendously deep and the number of inducing points dominates the dimension of output from each layer, then the distance between $f^{(H)}$ and $\mathcal{T}^{(H)}$ is relatively close. DGP $f^{(H)}$ is, in fact, an infinite-dimensional non-parametric model while DTMGP $\mathcal{T}^{(H)}$ is a parametrized model with finitely many parameters. Therefore, theorem 6 partially reflects that DTMGP can also well approximate other complex stochastic systems.

References

- Ankenman, B., B. L. Nelson, and J. Staum (2010). Stochastic kriging for simulation metamodeling. *Oper. Res.* 58(2), 371–382.
- Avramidis, A. N. and J. R. Wilson (1996). Integrated variance reduction strategies for simulation. *Operations Research* 44(2), 327–346.
- Banerjee, S., A. E. Gelfand, A. O. Finley, and H. Sang (2008). Gaussian predictive process models for large spatial data sets. *Journal of the Royal Statistical Society: Series B (Statistical Methodology)* 70(4), 825–848.
- Baydin, A. G., B. A. Pearlmutter, A. A. Radul, and J. M. Siskind (2018). Automatic differentiation in machine learning: A survey. *Journal of Machine Learning Research* 18(153), 1–43.

- Blei, D. M., A. Kucukelbir, and J. D. McAuliffe (2017, Apr). Variational inference: A review for statisticians. *Journal of the American Statistical Association* 112(518), 859–877.
- Blundell, C., J. Cornebise, K. Kavukcuoglu, and D. Wierstra (2015). Weight uncertainty in neural network. In *International Conference on Machine Learning*, pp. 1613–1622. PMLR.
- Bui, T., D. Hernandez-Lobato, J. Hernandez-Lobato, Y. Li, and R. Turner (2016, 20–22 Jun). Deep Gaussian processes for regression using approximate expectation propagation. Volume 48 of *Proceedings of Machine Learning Research*, New York, New York, USA, pp. 1472–1481. PMLR.
- Bungartz, H.-J. and M. Griebel (2004). Sparse grids. *Acta Numerica* 13, 147–269.
- Cressie, N. and G. Johannesson (2008). Fixed rank kriging for very large spatial data sets. *Journal of the Royal Statistical Society: Series B (Statistical Methodology)* 70(1), 209–226.
- Cutajar, K., E. V. Bonilla, P. Michiardi, and M. Filippone (2017, 06–11 Aug). Random feature expansions for deep Gaussian processes. Volume 70 of *Proceedings of Machine Learning Research*, International Convention Centre, Sydney, Australia, pp. 884–893. PMLR.
- Dai, B., B. Xie, N. He, Y. Liang, A. Raj, M.-F. F. Balcan, and L. Song (2014). Scalable kernel methods via doubly stochastic gradients. In Z. Ghahramani, M. Welling, C. Cortes, N. D. Lawrence, and K. Q. Weinberger (Eds.), *Advances in Neural Information Processing Systems* 27, pp. 3041–3049. Curran Associates, Inc.
- Dai, Z., A. Damianou, J. González, and N. Lawrence (2016). Variational auto-encoded deep Gaussian processes. *Proceedings of the International Conference on Learning Representations (ICLR) 2016*.
- Damianou, A. and N. Lawrence (2013). Deep Gaussian processes. Volume 31 of *Proceedings of Machine Learning Research*, Scottsdale, Arizona, USA, pp. 207–215. PMLR.
- Deng, L. (2012). The MNIST database of handwritten digit images for machine learning research. *IEEE Signal Processing Magazine* 29(6), 141–142.
- Ding, L., R. Tuo, and S. Shahrampour (2020). Generalization guarantees for sparse kernel approximation with entropic optimal features. In *International Conference on Machine Learning*, pp. 2545–2555. PMLR.
- Ding, L. and X. Zhang (2020). Sample and computationally efficient simulation metamodeling in high dimensions. *arXiv preprint arXiv:2010.06802*.
- Fei, J., J. Zhao, S. Sun, and Y. Liu (2018). Active learning methods with deep Gaussian processes. In *International Conference on Neural Information Processing*, pp. 473–483. Springer.
- Glorot, X., A. Bordes, and Y. Bengio (2011, 11–13 Apr). Deep sparse rectifier neural networks. Volume 15 of *Proceedings of Machine Learning Research*, Fort Lauderdale, FL, USA, pp. 315–323. JMLR Workshop and Conference Proceedings.

- Graves, A. (2011). Practical variational inference for neural networks. In J. Shawe-Taylor, R. S. Zemel, P. L. Bartlett, F. Pereira, and K. Q. Weinberger (Eds.), *Advances in Neural Information Processing Systems 24*, pp. 2348–2356. Curran Associates, Inc.
- Hastie, T., R. Tibshirani, and J. Friedman (2009). *The Elements of Statistical Learning: Data Mining, Inference, and Prediction* (2 ed.). Springer.
- Havasi, M., J. M. Hernández-Lobato, and J. J. Murillo-Fuentes (2018). Inference in deep Gaussian processes using Stochastic Gradient Hamiltonian Monte Carlo. In S. Bengio, H. Wallach, H. Larochelle, K. Grauman, N. Cesa-Bianchi, and R. Garnett (Eds.), *Advances in Neural Information Processing Systems*, Volume 31. Curran Associates, Inc.
- Hebbal, A., L. Brevault, M. Balesdent, E.-G. Talbi, and N. Melab (2021). Bayesian optimization using deep Gaussian processes with applications to aerospace system design. *Optimization and Engineering* 22(1), 321–361.
- Hensman, J. and N. D. Lawrence (2014). Nested variational compression in deep Gaussian processes.
- Hinton, G. (2010). A practical guide to training restricted Boltzmann machines (version 1). *Technical Report UTML TR 2010-003, University of Toronto* 9.
- Hinton, G., S. Osindero, and Y.-W. Teh (2006, 08). A fast learning algorithm for deep belief nets. *Neural Computation* 18, 1527–54.
- Katzfuss, M. and J. Guinness (2021). A general framework for vecchia approximations of gaussian processes. *Statistical Science* 36(1), 124–141.
- Ko, J. and H. Kim (2021). Deep Gaussian process models for integrating multifidelity experiments with non-stationary relationships. *IISE Transactions* (just-accepted), 1–28.
- Li, Y., S. Rao, A. Hassaine, R. Ramakrishnan, D. Canoy, G. Salimi-Khorshidi, M. Mamouei, T. Lukasiewicz, and K. Rahimi (2021). Deep Bayesian Gaussian processes for uncertainty estimation in electronic health records. *Scientific Reports* 11(1), 1–13.
- MacKay, D. J. (1992). A practical Bayesian framework for backpropagation networks. *Neural Computation* 4(3), 448–472.
- Marcus, M. B. and J. Rosen (2006). *Markov Processes, Gaussian Processes, and Local Times*. Cambridge University Press.
- Marmin, S. and M. Filippone (2022). Deep gaussian processes for calibration of computer models. *Bayesian Analysis* 1(1), 1–30.
- Matheron, G. (1963). Principles of geostatistics. *Econ. Geol.* 58(8), 1246–1266.
- Neal, R. M. (1996). *Bayesian learning for neural networks*, Volume 118. Springer Science & Business Media.
- Neidinger, R. D. (2010). Introduction to automatic differentiation and matlab object-oriented programming. *SIAM review* 52(3), 545–563.

- Pasupathy, R. and S. G. Henderson (2011). Simopt: A library of simulation optimization problems. In *Proceedings of the 2011 Winter Simulation Conference (WSC)*, pp. 4075–4085.
- Plumlee, M. (2014). Fast prediction of deterministic functions using sparse grid experimental designs. *J. Amer. Statist. Assoc.* 109(508), 1581–1591.
- Plumlee, M. (2021). Sparse grid designs. <https://www.mathworks.com/matlabcentral/fileexchange/45668-sparse-grid-designs>. MATLAB Central File Exchange.
- Plumlee, M. and R. Tuo (2014). Building accurate emulators for stochastic simulations via quantile kriging. *Technometrics* 56(4), 466–473.
- Radaideh, M. I. and T. Kozłowski (2020). Surrogate modeling of advanced computer simulations using deep Gaussian processes. *Reliability Engineering & System Safety* 195, 106731.
- Rahimi, A. and B. Recht (2008). Random features for large-scale kernel machines. In *Advances in Neural Information Processing Systems*, pp. 1177–1184.
- Ritter, K. (2000). *Average-case analysis of numerical problems*. Number 1733. Springer Science & Business Media.
- Sacks, J., S. B. Schiller, and W. J. Welch (1989). Designs for computer experiments. *Technometrics* 31(1), 41–47.
- Salimbeni, H. and M. Deisenroth (2017). Doubly stochastic variational inference for deep Gaussian processes. In I. Guyon, U. V. Luxburg, S. Bengio, H. Wallach, R. Fergus, S. Vishwanathan, and R. Garnett (Eds.), *Advances in Neural Information Processing Systems*, Volume 30. Curran Associates, Inc.
- Sauer, A., A. Cooper, and R. B. Gramacy (2022). Vecchia-approximated deep gaussian processes for computer experiments.
- Sauer, A., R. B. Gramacy, and D. Higdon (2022). Active learning for deep gaussian process surrogates. *Technometrics*, 1–15.
- Schmidt, W. F., M. A. Kraaijveld, and R. P. Duin (1992). Feedforward neural networks with random weights. In *Pattern Recognition, 1992. Vol. II. Conference B: Pattern Recognition Methodology and Systems, Proceedings., 11th IAPR International Conference on*, pp. 1–4. IEEE.
- Sidén, P. and F. Lindsten (2020). Deep Gaussian Markov random fields. In *International Conference on Machine Learning*, pp. 8916–8926. PMLR.
- Stein, M. L. (2014). Limitations on low rank approximations for covariance matrices of spatial data. *Spatial Statistics* 8, 1–19.
- Tran, D., R. Ranganath, and D. M. Blei (2016). The variational Gaussian process. *Proceedings of the International Conference on Learning Representations (ICLR) 2016*.

- van Dam, E. R., B. Husslage, D. den Hertog, and H. Melissen (2007). Maximin Latin hypercube designs in two dimensions. *Oper. Res.* 55(1), 158–169.
- Vecchia, A. V. (1988). Estimation and model identification for continuous spatial processes. *Journal of the Royal Statistical Society: Series B (Methodological)* 50(2), 297–312.
- Wang, W., R. Tuo, and C. F. J. Wu (2020). On prediction properties of kriging: Uniform error bounds and robustness. *J. Amer. Statist. Assoc.* 115(530), 920–930.
- Yang, J. and D. Klabjan (2021). Bayesian active learning for choice models with deep Gaussian processes. *IEEE Transactions on Intelligent Transportation Systems* 22(2), 1080–1092.